Atmos. Chem. Phys., 24, 14045–14072, 2024
https://doi.org/10.5194/acp-24-14045-2024

Atmospheric Chemistry and Physics
Open Access
EGU

High ice-nucleating particle concentrations associated with Arctic haze in springtime cold-air outbreaks

Erin N. Raif[1], Sarah L. Barr[1,2], Mark D. Tarn[1], James B. McQuaid[1], Martin I. Daily[1], Steven J. Abel[4], Paul A. Barrett[4], Keith N. Bower[3], Paul R. Field[1,4], Kenneth S. Carslaw[1], and Benjamin J. Murray[1]

[1]Institute for Climate and Atmospheric Science, School of Earth and Environment, University of Leeds, Woodhouse Road, Leeds, LS2 9JT, UK
[2]National Centre for Atmospheric Science, Clarendon Road, Leeds, LS2 9PH, UK
[3]Atmospheric Science Research Group, Department of Earth and Environmental Sciences, University of Manchester, Oxford Road, Manchester, M13 9PL, UK
[4]Met Office, FitzRoy Road, Exeter, EX1 3PB, UK

Correspondence: Erin N. Raif (eeenr@leeds.ac.uk)

Received: 21 May 2024 – Discussion started: 23 May 2024
Revised: 24 September 2024 – Accepted: 27 September 2024 – Published: 17 December 2024

Abstract. The global variation in ice-nucleating particle (INP) concentrations is an important modulator of the cloud-phase feedback, where the albedo of mixed-phase clouds increases in a warming climate. Shallow clouds, such as those observed in cold-air outbreaks (CAOs), are particularly important for cloud-phase feedbacks and highly sensitive to INPs. To investigate the sources and concentrations of INPs in CAOs, we made airborne measurements over the Norwegian and Barents seas as part of the March 2022 Arctic Cold-Air Outbreak (ACAO) field campaign. Aerosol samples were collected on filters at locations above, below and upstream of CAO cloud decks. Throughout the campaign, INP concentrations were comparable to the highest concentrations previously observed in the Arctic. Scanning electron microscopy analysis of samples taken upstream of cloud decks showed that supermicron aerosol was dominated by mineral dusts. Analysis of aerosol particle size measurements to obtain an INP active site density suggested sea spray was unlikely to be the dominant INP type. These site densities were also too great for mineral components alone to be the dominant INP type above −20 °C. Accordingly, it is likely that the dominant INP type was mineral dust mixed with other ice-nucleating materials, possibly of biogenic origin. Back-trajectory analysis and meteorological conditions suggested a lack of local INP sources. We therefore hypothesise that the high INP concentration is most likely to be associated with aged aerosol in Arctic haze that has undergone long-range transport from lower-latitude regions.

1 Introduction

Marine cold-air outbreaks (CAOs) are frequent high-intensity weather events in the mid- to high-latitudes where cold polar air is drawn equatorward over an increasingly warmer ocean (Fletcher et al., 2016b). The relative warmth of the ocean compared to the air mass causes the polar air to become warmer and more moist, resulting in extensive mixed-phase cloud systems (Brümmer, 1996; Fletcher et al., 2016a; Abel et al., 2017). In these cloud systems, stratiform clouds form at the sea-ice edge, which transition into open cumulus cells as the air mass moves equatorward. These often take the form of "cloud streets", streaks of stratocumulus clouds in the direction of the prevailing wind (Pithan et al., 2018; Murray-Watson et al., 2023).

The presence of supercooled liquid water in these mixed-phase CAO clouds makes them sensitive to the presence of ice-nucleating particles (INPs). INPs are a subset of aerosol that allow droplets of supercooled liquid water in clouds to freeze at temperatures above −35 °C (Murray et al., 2012b; Kanji et al., 2017), where homogeneous freezing does not occur at appreciable rates (Ickes et al., 2015; Herbert et al.,

2015). Globally significant INP species include mineral dust, sea-spray aerosol, and biological material such as bacteria and fungal spores (Kanji et al., 2017). Where ice and liquid coexist in mixed-phase clouds, ice particles are able to grow by vapour deposition at the expense of liquid droplets since the saturation vapour pressure over liquid is greater than the saturation vapour pressure over ice (Wegener, 1911). Through this process, ice crystals are able to grow to sizes at which they can precipitate, enhancing precipitation (Bergeron, 1935; Findeisen, 1938). Since ice crystal concentrations are typically lower than liquid droplet concentrations in mixed-phase clouds, this process can be highly efficient. Ice crystals that have formed through ice nucleation may also grow via subsequent microphysical processes such as riming, where supercooled droplets are collected by ice crystals. Additionally, the ice crystal concentration may increase through secondary ice processes such as rime splintering (Field et al., 2017; Hallett and Mossop, 1974; Korolev and Leisner, 2020). Consequently, the concentration of INPs can act as a strong control on the ratio of liquid and ice in a mixed-phase cloud.

Since increased proportions of ice are associated with reduced albedo, the concentration of INPs can influence the albedo of the cloud (Garrett et al., 2001; Korolev et al., 2017). In simulations of a Southern Hemisphere CAO, Vergara-Temprado et al. (2018) showed that the reflectivity of clouds in CAO systems decreases with increasing INP concentration since low INP concentrations suppressed droplet freezing and precipitation and increased cloud lifetime. Additionally, simulations of a Northern Hemisphere CAO by Abel et al. (2017) showed that precipitation can influence the rate of cloud transition between the more reflective stratiform state and the less reflective cumuliform state, while simulations of CAOs by Tornow et al. (2021) showed that INPs can influence the onset of precipitation and thus the initiation of the reduction in cloud cover due to the cloud transition. In a warming climate, ice crystals in mixed-phase clouds will be susceptible to replacement by liquid water, increasing cloud albedo, thus resulting in a cooling feedback (Storelvmo et al., 2015). Since INP concentration can modulate the concentration of ice, the availability of INPs in CAO clouds could influence the magnitude of this cloud-phase feedback (Murray et al., 2021). The cloud-phase feedback is likely to be particularly sensitive to CAO clouds since they form over the relatively dark ocean, so microphysical adjustments to cloud albedo have the potential to be more impactful than for clouds over higher-albedo surfaces such as sea ice.

INP concentrations vary substantially both spatially and temporally, but some of the greatest variability observed anywhere on Earth occurs in the Arctic. Measurements of INPs in the Arctic reveal some of the lowest INP concentrations on Earth, comparable with the Southern Ocean, and some of the greatest, comparable with mid-latitude locations where terrestrial biological INP types dominate (Murray et al., 2021). Variability occurs both on seasonal scales (Wex et al., 2019; Sze et al., 2023) and strongly on timescales of hours to days (Porter et al., 2022). This indicates not only that the sources of INPs within and transported to the Arctic are variable, but also that removal processes are important, since periods of high INP concentration can be followed by periods of low INP concentration.

Figure 1a shows the potential sources of INPs for CAO clouds in the Northern Hemisphere. Potential Arctic sources of INPs are biogenic material from sea-spray (Wilson et al., 2015; DeMott et al., 2016; McCluskey et al., 2018b) and terrestrial INPs from high-latitude sources (Kawai et al., 2023). Potential terrestrial sources of INPs include glacial outwash sediments (Tobo et al., 2019; Xi et al., 2022; Barr et al., 2023), sandy deserts in Iceland (Sanchez-Marroquin et al., 2020), boreal forests (Brasseur et al., 2022), Arctic surface vegetation (Pereira Freitas et al., 2023) and thawing permafrost (Creamean et al., 2020). In addition, Arctic aerosol can have lifetimes of many weeks, which results in the build up of Arctic haze in winter and spring (Stohl, 2006). Accordingly, it is also possible that INPs entering CAOs may have been transported into the Arctic from lower latitudes where they reside in the stable Arctic atmosphere before being transported out again in CAOs (Carslaw, 2022). Different types of INPs have different characteristic ranges of freezing temperatures (Kanji et al., 2017). This means understanding the aerosol sources that contribute to the INP population in CAO clouds can reduce the uncertainty in the cloud-phase feedback.

To understand the sources of INPs in CAO clouds, there is a need for localised airborne aerosol measurements to capture INP concentrations throughout a cold-air outbreak, especially in the Northern Hemisphere. Previously, Northern Hemisphere aircraft campaigns have characterised the dynamics of cold-air outbreaks (Brümmer, 1996) over the Norwegian Sea and have made airborne measurements of aerosol and clouds without INP measurements in mid-latitude cold-air outbreak conditions (Young et al., 2016; Sorooshian et al., 2019). INP measurements have been made in CAOs from the ground in the Northern Hemisphere (Geerts et al., 2022; Gjelsvik et al., 2024) and from aircraft in the Southern Hemisphere (McFarquhar et al., 2021; McCluskey et al., 2018a). In this study, we focus on cold-air outbreaks over the Norwegian and Barents seas to report the first airborne measurements of INPs in Northern Hemisphere cold-air outbreaks. Having reported these measurements, we characterise the INP concentrations observed and try to identify the primary INP source(s) through a process of elimination of potential sources.

2 Methodology

2.1 The Arctic Cold-Air Outbreak campaign

The Arctic Cold-Air Outbreak (ACAO) flight campaign took place over the Norwegian and Barents seas in March 2022. The campaign used the BAe 146 aircraft of the Facility for

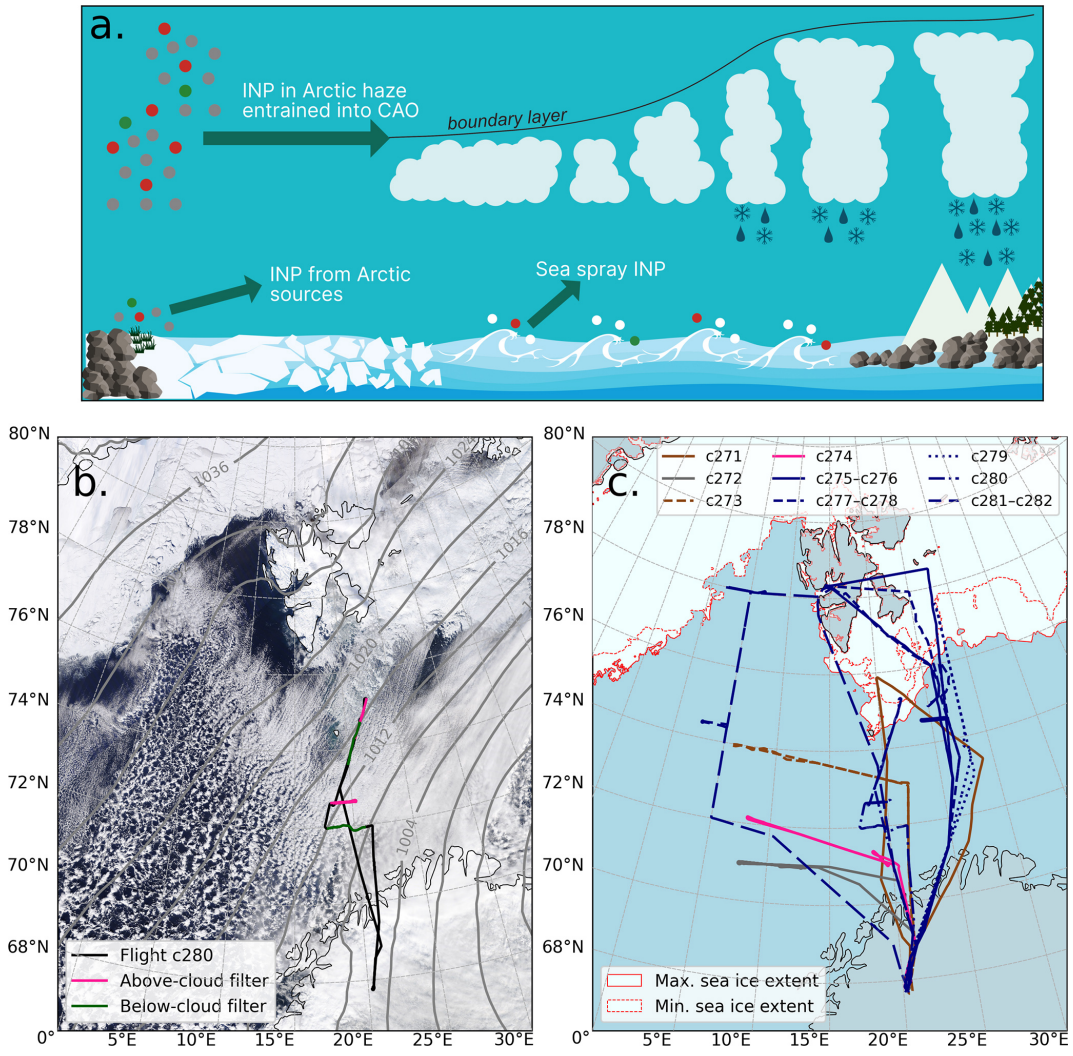

Figure 1. Panel **(a)** shows a schematic representation of an Arctic cold-air outbreak and potential sources of aerosol to the cloud system. The green and red circles depict biological and abiological INPs respectively, while the grey and white circles depict aerosols that do not nucleate ice in CAOs. Panel **(b)** shows satellite imagery taken on 29 March 2022 by the Moderate Resolution Imaging Spectroradiometer (MODIS) of a typical CAO measured during the ACAO campaign (MODIS Land Science Team, 2020). The path of flight c280, which probed this CAO, is overlaid along with the locations of INP filter samples, which were taken between 30 min and 2 h before the image time. Sea-level pressure isobars from ERA5 reanalysis are also overlaid (C3S, 2018). Panel **(c)** shows the flight paths from all 9 flying days during the campaign. The blue, pink and brown flight paths represent CAOs with predominantly N, NW and W flows respectively. Flight c272 probed a warm-air intrusion and is coloured grey. Sea-ice extent in this and other maps was obtained from the Multisensor Analyzed Sea Ice Extent dataset (U.S. National Ice Center et al., 2010). The flight track for flight c278 is incomplete due to equipment failure.

Airborne Atmospheric Measurements (FAAM) to make measurements in cold-air outbreaks. A key aim was to investigate the development and evolution of the cloud systems and the associated aerosol and cloud microphysical properties. A total of 12 flights were performed over 9 d between 11 and 30 March 2022. The tracks of these flights are depicted in Fig. 1c. Where possible, flight days and locations were chosen to capture cold-air outbreaks with characteristics such as cloud streets that were clearly positioned away from fronts to ensure well-defined air flows and air masses. CAO conditions, of varying strength, occurred on 8 of the 9 flying days. On the other day (flight c272), a warm-air intrusion (an injection of mid-latitude air into the Arctic; Pithan et al., 2018) occurred and was measured as a contrasting case. Flights c271 and c273 probed CAOs with westerly flows with air flowing off Greenland, while the flow during c274 was northwesterly. Flights c275 to c282 probed CAOs with northerly or north by northeasterly flows. Aerosol measurements were made online (i.e. continuously) using underwing optical probes, and filter samples were collected for specific periods for subsequent offline analysis.

2.2 Filter samples for INP analysis

In this system, filter samples were collected using the aircraft inlet system characterised by Sanchez-Marroquin et al. (2019). Two parallel inlets are aligned with the heading of the aircraft, and the airflow through each inlet is assisted by a vacuum pump. The inlet system is designed to minimise turbulence and flow separation when flying at a low Mach number (Andreae et al., 1988, 2000) and has a bypass to remove droplets and ice crystals (Talbot et al., 1990). The bypass also increases the flow rate, reducing the sub-isokinetic enhancement of larger particles (Sanchez-Marroquin et al., 2019). A different type of filter was used in each inlet so that different types of analyses could be performed on aerosol samples from the same location and time. Polytetrafluoroethylene (PTFE) membrane filters were used for INP concentration measurements via droplet-freezing assays, while polycarbonate track-etched membrane filters were used for scanning electron microscopy with energy-dispersive X-ray spectroscopy (SEM-EDS) aerosol composition analysis.

Air entering each inlet passes through a sampling line into a filter holder previously described by Price et al. (2018) and Sanchez-Marroquin et al. (2019). Air that passes through the filter holder is measured by a mass flow meter, which reports the flow in standard litres (273.15 K, 101.325 kPa). Inside the filter holder, the filter sits on a stainless steel support mesh. The PTFE filter (Sartorius, product number 11803-47-N) has a pore size of 1.2 µm, while the polycarbonate filter (Whatman, product number 111107) has a pore size of 0.4 µm. The PTFE filter allowed more throughput for INP analysis, while the polycarbonate filter had less throughput. Two types of steel mesh were used during the campaign – one manufactured by Millipore (product number XX4304707) and one manufactured by MesaLabs (product number 1584). Using the MesaLabs meshes enhanced the flow through the filter, though flow rates were consistently greater through PTFE filters than through polycarbonate filters. Flow through the filter was also dependent on altitude, with higher flow rates at lower altitudes. The largest volume of air sampled by a PTFE filter was (1730 ± 30) L, while the smallest volume of air sampled was (473 ± 9) L. For polycarbonate filters, the largest volume sampled was (990 ± 20) L, while the smallest was (276 ± 6) L. There was no correlation between the INP concentrations measured and the volume of air sampled by each filter. Handling blanks were collected to determine the baseline ice-nucleating activity of the procedure and equipment used. These handling blanks were collected during the flight by loading filters as normal into the aircraft filter holder system, opening the filter system up to air flow for 1–2 s, then closing the filter system and removing the filters as normal. Handling blank filters were processed for INP analysis in the same manner as the aerosol sample filters.

Figure 2a shows the location of the filter sample measurements over the Norwegian and Barents seas between 71–79° N. The altitude of filter measurements was between 40–3400 m, and all samples were taken in air with no clouds or precipitation. The majority of samples were taken above or below the CAO clouds, although two samples (c276r2 and c278r2) were taken upstream of the cloud onset. Sampling periods were typically between 18–28 min, excluding pauses in sampling where the inlets were temporarily closed when the aircraft turned or flew through precipitation. Only one of the samples (c273r2) had a shorter sampling time of 14 min, while one of the samples (c273r1) had a longer sampling time of 37 min. However, both of these filters sampled volumes of air that were not at the extremities of the volume range sampled.

To derive INP concentrations from the samples, droplet-freezing assays were performed according to a drop-on technique described fully by Price et al. (2018), which makes use of the microlitre Nucleation by Immersed Particle Instrument (Whale et al., 2015). Filters were processed in a field laboratory set up in a hotel room to minimise the storage and transport effects that are known to lead to loss of INPs (Beall et al., 2020). All but one of the filters were processed within 24 h of collection. In these experiments, rectangular glass cover slips (48 mm × 64 mm, no. 1.5 thickness, Agar Scientific, UK) were washed with purified water (high-performance liquid chromatography grade, Sigma-Aldrich, UK) and isopropanol (VWR, UK) and then immersed for 1 h in a petri dish containing Turtle Wax ClearVue rain repellent solution (Rapid Electronics, UK) to render them hydrophobic. The slides were removed from the ClearVue solution, rinsed with isopropanol and water, and then dried with particle-free air from an oil-free air compressor (24 L, model HY7524, Hyundai, UK, with a HEPA filter in line). In a laminar flow hood, a filter onto which aerosol had been sampled was placed onto a hydrophobic slide, and between 60 and 70 droplets of purified water with a volume of 2 µL were pipetted directly onto the filter using a manual electronic pipette. The hydrophobic glass slide–filter assembly was then placed onto a cold plate of an Asymptote EF600 Stirling engine-based cold stage with a drop of silicone oil in between to aid thermal contact. A flow of HEPA-filtered compressed air that had been passed through a drying column (Drierite 26800, Sigma-Aldrich, UK) was used to flush the volume above the droplets to prevent frost formation. The filter was then cooled at a rate of 1 K min^{-1} until all droplets froze. The cooling was recorded by a camera, and the temperature of the cold plate was measured concurrently. Software written in Python was used to automatically detect freezing events and determine the temperature at which each droplet froze (Barr, 2023). The same procedure was used for handling blanks from the aircraft. In addition, filter blanks were run each day, consisting of purified water droplets pipetted onto new, untouched filters to ensure that the procedure and equipment were operating correctly and without unacceptable contamination (or that the system was cleaned and procedures were improved until contamination levels were deemed acceptable).

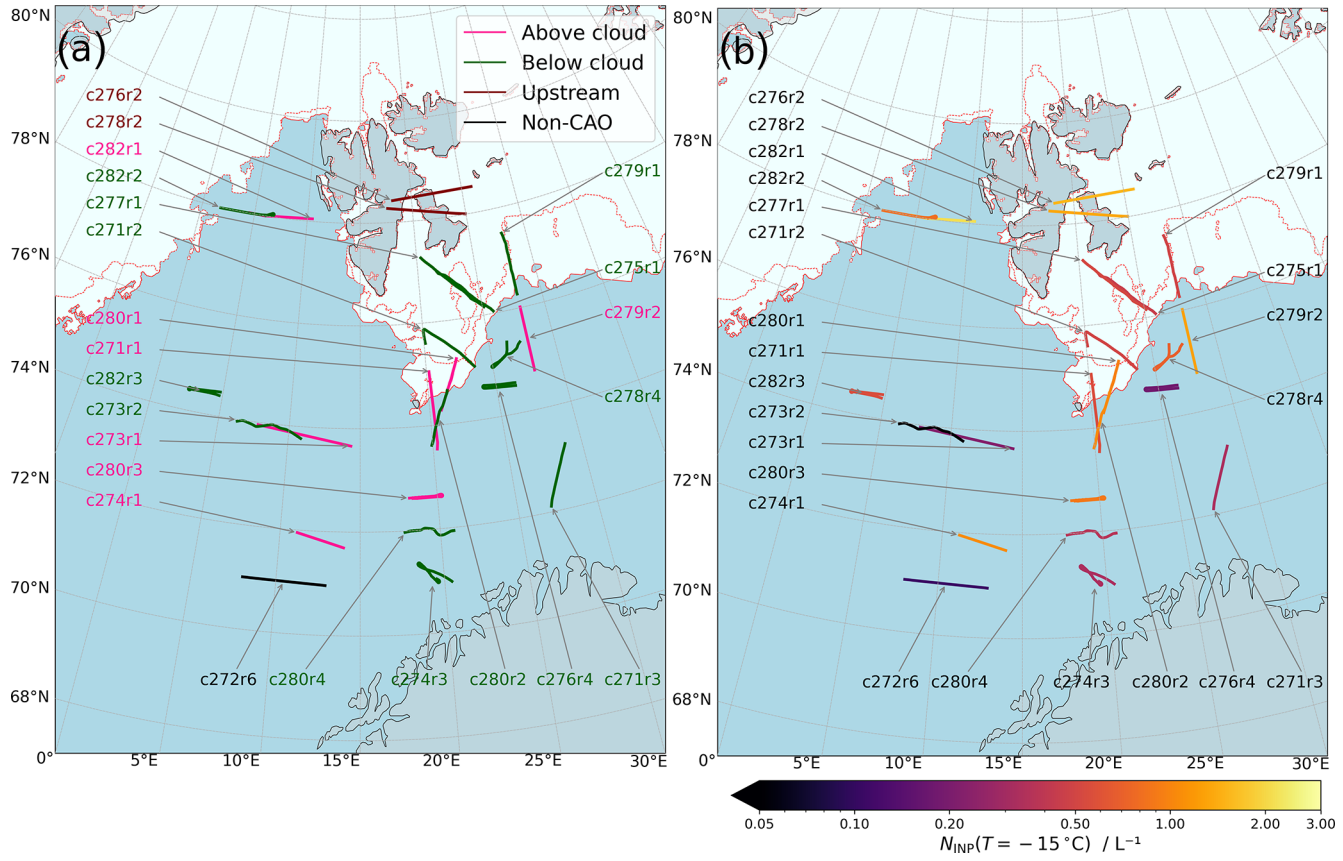

Figure 2. Locations of all filter samples taken during the ACAO campaign. Panel **(a)** displays the location of the sample relative to the cloud deck, while panel **(b)** shows $N_{INP}(-15\,°C)$, the INP concentration at $-15\,°C$ for each sample. All filters except c272r6 were taken in CAO conditions.

An alternative assay technique is to wash aerosol material off the filters in a larger volume of deionised water and take microlitre droplets from this volume for freezing experiments (O'Sullivan et al., 2018). Given the relatively short collection time for aerosols on the filters, the drop-on technique was chosen because it utilises a greater fraction of aerosols collected during the sampling period (approximately 30 times more aerosol per droplet). This gives greater sensitivity to the relatively small fraction of all aerosols that are able to nucleate ice (Sanchez-Marroquin et al., 2021). Using filters collected in parallel, comparison between the wash-off and drop-on techniques shows good agreement in the INP concentration ranges where the techniques overlap (Sanchez-Marroquin et al., 2021). However, in one-third of cases compared by Sanchez-Marroquin et al. (2021), the wash-off technique produced lower INP concentrations at temperatures above $T = -20\,°C$, temperatures at which biological and biologically enhanced INPs are active. The wash-off technique agrees well with other online and offline INP analysis techniques for mineral dusts (DeMott et al., 2018) but produced lower INP concentrations for a cellulose sample compared to other techniques (Hiranuma et al., 2019). Similarly, the wash-off technique produced lower INP concentrations than a liquid impinger technique when measuring INPs in the Arctic, which was attributed to the larger size cut-off of the impinger technique (Li et al., 2023).

From droplet-freezing temperatures, INP temperature spectra were derived using the framework of Vali (1971, 2019). For each assay, freezing events were grouped into temperature bins with a size of $\Delta T = 1\,K$ to calculate the differential nucleus spectrum,

$$k_{assay}(T) = -\frac{1}{V_d \Delta T} \ln\left(1 - \frac{\Delta N}{n(T)}\right), \quad (1)$$

where V_d is the droplet volume (2 µL), ΔN is the number of droplets that freeze in a temperature interval and $n(T)$ is the number of droplets unfrozen at T, the upper limit of the bin's temperature range. The error in ΔN according to the Poisson distribution was propagated to find the error in $k_{assay}(T)$ for the individual spectrum. The average differential INP spectrum of the background filters, k_{bg}, was subtracted from the spectra for an individual assay to get the "true" differential INP spectrum for a sample,

$$k(T) = k_{assay}(T) - k_{bg}(T). \quad (2)$$

From this, the INP concentration, N_{INP}, was calculated as

$$N_{INP}(T) = \frac{V_d A_f}{V_a A_d} \Delta T \sum_{0}^{T} k(T), \quad (3)$$

where V_a is the volume of air sampled; A_f is the surface area of the filter exposed to aerosol, $(11 \pm 2)\,cm^2$; and A_d is the surface area of the filter in contact with a droplet, $(0.014 \pm 0.002)\,cm^2$. A_d was calculated using spherical cap geometry with a contact angle of 126° as in Price et al. (2018).

2.3 Scanning electron microscopy

Using the method described by Sanchez-Marroquin et al. (2019), SEM-EDS was used on two filters to ascertain the size-resolved elemental composition of aerosol captured on the polycarbonate filters. The elemental composition was used to estimate the fraction of aerosol from terrestrial dust and marine sources. Portions of the filters were mounted on 25 mm diameter stubs, sputter-coated with 30 nm of platinum and analysed at the University of Leeds with a Tescan Vega3 XM electron microscope fitted with an Oxford Instruments X-Max 150 SDD (silicon drift detector) energy-dispersive X-ray spectrometer. Using AZtec 3.3 feature recognition software, the filters were scanned for aerosol particles, and a prescribed algorithm was used to automatically classify particles into categories (e.g. mineral dust and sea spray) using their elemental composition. This classification algorithm is further described in Sanchez-Marroquin et al. (2019). The carbonaceous category of particles includes particles which contain no elements other than O and C and therefore does not distinguish between organic and elemental carbon. Biological particles are therefore not explicitly classified using this method but can be qualitatively identified on the basis of size and morphology (Sanchez-Marroquin et al., 2021). The classified particles were then binned according to their equivalent spherical diameter. A minimum diameter of 0.3 µm was chosen as it is comfortably above the size threshold at which the feature recognition software erroneously detects features. The total surface area of aerosol sampled in each composition category was normalised by the fraction of filter area analysed and the volume of air sampled during the sampling run.

2.4 Optical probes

Two underwing optical probes were used to measure the aerosol number, surface area and volume concentrations during the flight. These were the Passive Cavity Aerosol Spectrometer Probe (PCASP) 100X (Droplet Measurement Technologies with SPP200 electronics) and Cloud Droplet Probe (CDP; Droplet Measurement Technologies). Both probes operate by measuring the intensity of radiation from a laser that is scattered by incident particles. For the CDP, sampled particles pass directly through the beam, while for the PCASP, a sample is enclosed in clean air before entering an optical chamber. Both probes use the magnitude of the scattered radiation to assign the particle to 1 of 30 bins associated with the diameter of the particle (Rosenberg et al., 2012). Although the CDP is designed to measure droplets, it has previously been used to measure coarse-mode aerosol by adjusting the calibration of the probe to assume a refractive index representative of the aerosol sampled (Sanchez-Marroquin et al., 2020). To do this, the calibration method of Rosenberg et al. (2012) was used to calculate the particle diameters measured by each bin when given a refractive index. For this study, particle size distributions were first obtained using real refractive indices ranging from 1.5–1.7 and imaginary components ranging from 0–0.003i as in Sanchez-Marroquin et al. (2020). Since the error associated with the refractive index was small, a refractive index value of 1.56+0i was chosen for consistency with Sanchez-Marroquin et al. (2020). When using a refractive index of 1.56, the PCASP measures particles with a diameter range of 0.1–3 µm, while the CDP measures particles with a diameter range of 4.5–70 µm.

Previous studies have found that the coarse-mode aerosol number reported by the PCASP and CDP probes is suppressed relative to particles counted on filter samples using SEM (Sanchez-Marroquin et al., 2019; Barr, 2023). The use of larger-pore filters and a fully open bypass line (as described in Sect. 2.2) minimised this discrepancy.

To ensure that no cloud droplets or swollen hygroscopic aerosol was reported by the CDP, CDP data have only been used when relative humidity was below 80 % and when cloud-free air was identified using the Nevzorov hot-wire instrument. The Nevzorov instrument derives the liquid and total condensed water content (liquid and ice) based on the power required to melt and evaporate hydrometeors collected by the instrument (Korolev et al., 1998; Abel et al., 2014). The power supplied to the Nevzorov probe is significantly different in and out of the cloud. Using this variation in power supply, a 1 Hz cloud flag was derived to partition the data as in or out of the cloud in a manner similar to Barrett et al. (2020).

3 Results

Successful INP analysis was performed on 23 filter samples. All but filter c272r6 were taken when mixed-phase boundary layer clouds associated with cold-air outbreaks were present. A total of 13 samples were taken above the cloud deck, 8 were taken below the cloud deck and 2 were taken upstream of the development of the cloud in clear air. These sampling locations were considered to represent air below, above and before the development of the atmospheric boundary layer over sea respectively. The locations, altitudes and purpose of each filter measurement are shown in Table 1. Figure 2a shows that the filter samples were distributed throughout the development of the cold-air outbreaks.

Table 1. Times, locations and sampling intent of all filter samples made during the campaign.

Sample ID	Run type	Date (yyyy-mm-dd)	Start (UTC)	End (UTC)	Mean altitude (m)	Mean latitude (° N)	Mean longitude (° E)	CAO flow	Notes
c271r1	above cloud	2022-03-11	09:40:07	10:07:24	1747	74.3	20.3	W	
c271r2	below cloud	2022-03-11	10:18:03	10:42:48	39	75.5	21.5	W	2 min pause during aircraft turning
c271r3	below cloud	2022-03-11	11:18:05	11:38:38	49	72.7	27.9	W	filter processed 3 d after collection two pauses for precipitation
c272r6	above cloud	2022-03-16	12:07:25	12:34:15	2957	71.0	10.5	N/A	warm-air intrusion conditions
c273r1	above cloud	2022-03-19	12:01:25	12:38:51	3403	73.8	11.2	W	
c273r2	below cloud	2022-03-19	12:54:07	13:13:35	415	73.9	8.7	W	two short pauses to avoid showers
c274r1	above cloud	2022-03-21	13:47:10	14:07:23	2672	71.8	12.6	NW	
c274r3	below cloud	2022-03-21	15:18:08	15:41:22	165	71.2	19.3	NW	two short pauses for aircraft turning and one pause to avoid showers
c275r1	below cloud	2022-03-23	10:03:37	10:28:22	162	76.5	23.8	N	
c276r2	upstream	2022-03-23	12:55:29	13:20:29	1711	78.5	22.0	N	
c276r4	below cloud	2022-03-23	14:32:27	14:55:27	156	74.6	25.2	N	
c277r1	below cloud	2022-03-24	10:30:52	10:59:06	159	76.7	22.8	N	two pauses for altitude increases due to poor visibility cloud was in the very early stages of formation
c278r2	upstream	2022-03-24	13:02:05	13:26:16	1725	78.2	21.3	N	
c278r4	below cloud	2022-03-24	14:07:00	14:31:56	333	75.1	26.0	N	2 min pause during aircraft turning due to precipitation
c279r1	below cloud	2022-03-25	11:23:21	11:44:12	155	76.9	28.0	N	
c279r2	above cloud	2022-03-25	11:48:26	12:08:44	1323	75.4	28.0	N	
c280r1	above cloud	2022-03-29	09:29:00	09:49:17	1573	74.8	21.6	N	
c280r2	below cloud	2022-03-29	09:59:55	10:15:58	327	74.1	20.6	N	
c280r3	above cloud	2022-03-29	10:34:01	10:54:06	2013	72.6	19.4	N	2 min pause during aircraft turning
c280r4	below cloud	2022-03-29	11:05:35	11:24:51	334	72.0	19.3	N	1 min pause to avoid showers
c282r1	above cloud	2022-03-30	12:08:32	12:28:27	1761	78.0	7.5	N	
c282r2	below cloud	2022-03-30	12:40:23	13:01:59	308	78.0	4.6	N	brief pause for aircraft manoeuver the polycarbonate filter holder popped open and the filter was replaced 5 min into the run
c282r3	below cloud	2022-03-30	14:02:12	14:26:08	307	74.4	3.5	N	4 min pause during aircraft turning

3.1 INP concentration spectra

Figure 3a shows a composite of the INP concentration spectra ($N_{INP}(T)$) measured throughout the campaign. Measurements on and after 21 March (c274 onward, when the flows had a northerly component) form a tight band of INP spectra, all falling within about 1 order of magnitude and centred at about 1 L^{-1} at −15 °C. Spectra from 11 March through to 19 March (flights c271 to c273), when the flow directions were from the west or south, had much more variable INP concentrations, with one filter measurement recording an INP concentration below 0.1 L^{-1} at −15 °C (c273r2) (see Fig. A1). The median CAO INP concentration during the campaign, $\overline{N}_{INP}$, was described by the function

$$\overline{N}_{INP} = \overline{\nu}_{INP} \exp\left[\overline{a}\left(\overline{T}_{max} - T\right)^{\overline{b}}\right], \quad (4)$$

with fitting parameters $\overline{\nu}_{INP} = 1.480 \times 10^{-2}\,L^{-1}$, $\overline{T}_{max} = 226.2\,K$, $\overline{a} = 1.271\,K^{-0.5}$ and $\overline{b} = 0.5$. The fitting procedure used to obtain $\overline{N}_{INP}$ is described in Appendix B, along with similar four-parameter fits for each individual filter measurement. Figure 4 shows that INP concentrations during the ACAO campaign were among the highest recorded in the high latitudes of the Northern Hemisphere in springtime. They are comparable with the highest mid-latitude INP measurements collated by Petters and Wright (2015) and INP concentrations measured by Sanchez-Marroquin et al. (2020) in autumnal Icelandic dust plumes. They were also similar to the highest INP concentrations reported by Porter et al. (2022) at the North Pole in August 2018 when aerosol was transported from the Russian coast. Both Rogers et al. (2001) and Prenni et al. (2007) used an online thermal gradient diffusion chamber to quantify INPs from an aircraft north of Alaska during May and September–October respectively. While they often saw no detectable INPs, they also reported periods when INP concentrations were comparable to (or sometimes greater than) those found in ACAO. Sanchez-Marroquin et al. (2023) reported airborne INP measurements from March in northern Alaska using the same filter technique as used in ACAO, revealing INP concentrations at least 1–2 orders lower than in ACAO, with a steeper slope (many measurements were consistent with the background). These flights were not focused on CAO events.

The only previous airborne springtime INP measurements made in the vicinity of Svalbard were made by Hartmann et al. (2020), who flew over sea ice in the Arctic Ocean and Fram Straight in late March and early April 2018 and collected aerosol onto polycarbonate filters for a wash-off droplet-freezing assay. Hartmann et al. (2020) collected filter samples from an entire flight rather than in specific locations and reported INP concentrations that were 1–2 orders of magnitude lower than those observed during ACAO in three out of nine samples. The other six samples had lower INP concentrations, often consistent with their handling blanks. The three higher INP samples, which contained heat-sensitive INPs, were associated with airflows with a strong northerly component, and satellite imagery (MODIS Land Science Team, 2020) shows classic CAOs on these days. In contrast, the other samples were associated with less well-defined air mass trajectories that were not CAO events or, in one case, with a CAO event where the air originated from the west in the Canadian archipelago rather than the central Arctic.

Geerts et al. (2022) reported INP concentrations derived using the wash-off technique during CAOs from December 2019 to May 2020 at Andenes on the coast of northern Norway. The ground-based measurements at this downstream site revealed INP concentrations that were 2–3 orders of magnitude lower than in ACAO. This might be consistent with loss of INPs in the precipitating clouds in the CAO. Ground measurements of INP concentrations made during 2012 by Wex et al. (2019) in Ny-Ålesund (upstream of the CAO clouds in ACAO), using a quartz filter technique, were also 2–3 orders of magnitude lower than those observed during ACAO. However, the highest INP concentrations observed in this dataset occurred during summer rather than springtime. A similar seasonal dependence was also observed in the high Arctic by Creamean et al. (2022), who observed INP concentrations 2–4 orders of magnitude below those in the ACAO campaign during their year-round INP measurements. Creamean et al. (2022) used a technique that involved size selecting aerosols, impacting them onto petrolatum and then recovering these particles into water for a droplet-freezing assay. Ship-based measurements of INPs in the ocean around Svalbard, made with the wash-off technique between May and July 2017, were 1–2 orders of magnitude below those made during the ACAO campaign (Hartmann et al., 2021).

Rinaldi et al. (2021) used two offline methods to measure INP concentrations sampled at a ground-based site near Ny-Ålesund between April and August 2018. They found that using a dynamics filter processing chamber to measure INP concentration using condensation freezing yielded INP concentrations approximately 8 times greater than those yielded by a droplet-freezing assay measurement using a wash-off technique. However, the highest concentrations measured by Rinaldi et al. (2021) were lower than the lowest observed during ACAO and were typically 1–3 orders of magnitude below those measured in this campaign. Similarly, Li et al. (2023) used several different techniques to measure INPs at a Ny-Ålesund ground site during October and November 2019. These included an impinger sampling method, a continuous-flow diffusion chamber (CFDC) and a polycarbonate filter wash-off technique. These measurements had a much greater spread than those in ACAO and were typically 1–4 orders of magnitude lower. However, the measurement spread reduced at lower temperatures, and if extrapolated log-linearly, wash-off measurements were consistent with measurements made by the CFDC at $T = -30$ °C. Similarly, although the CFDC measurements were made at lower temperatures than

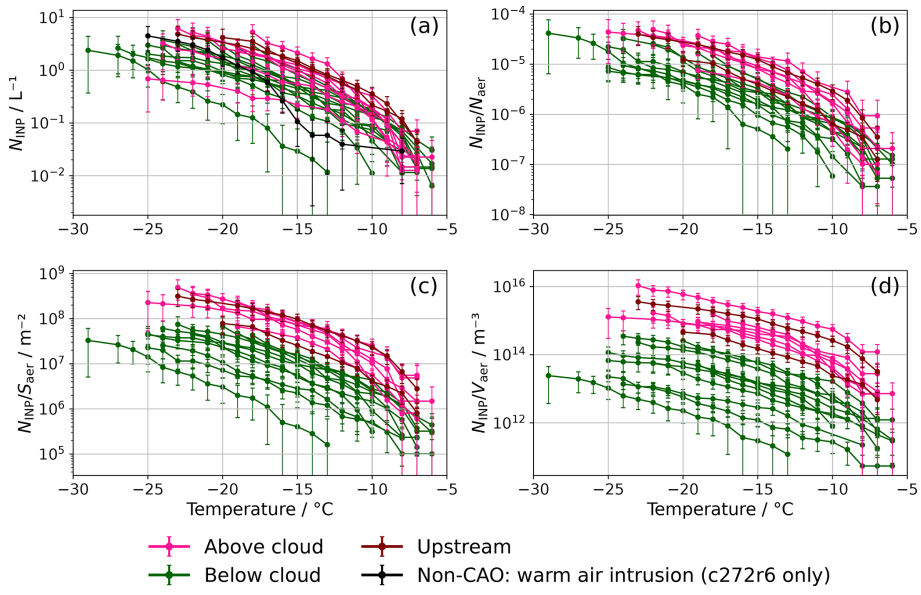

Figure 3. Panel **(a)** shows INP concentrations for each sample made during the campaign. Panels **(b)**, **(c)** and **(d)** show these concentrations normalised by the total number (N_{aer}), surface area (S_{aer}) and volume (V_{aer}) of aerosols with diameters greater than 0.1 µm. A version of this figure where each sample is individually labelled can be found in Appendix A.

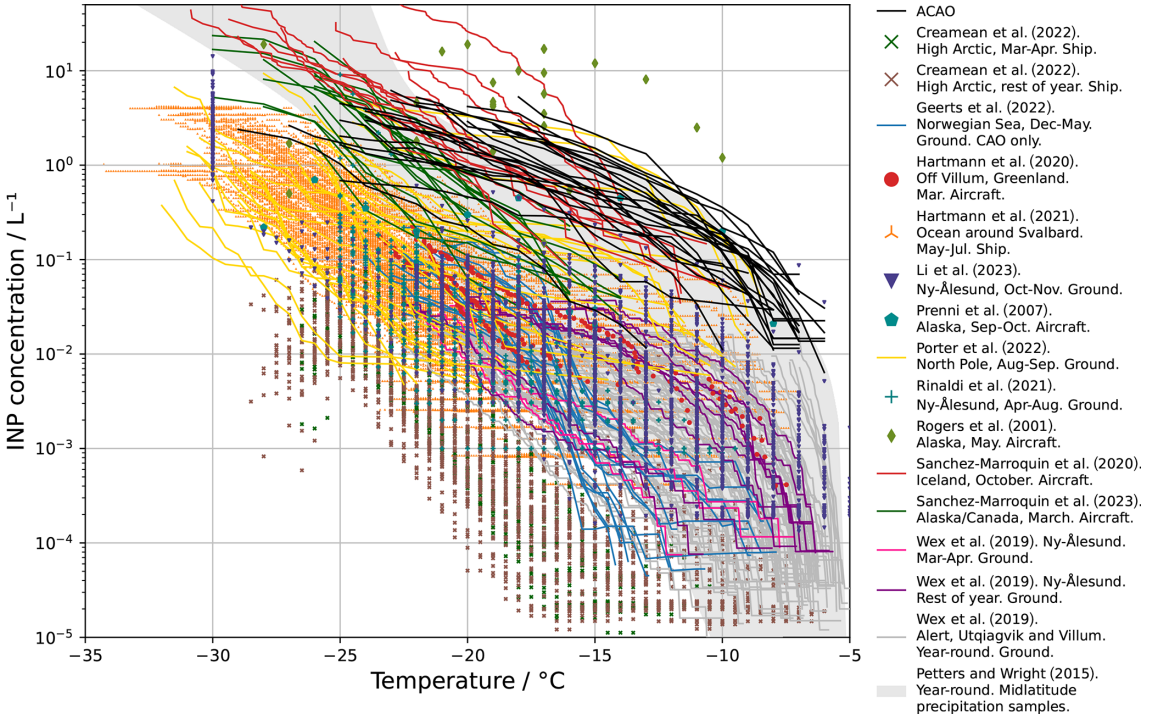

Figure 4. INP concentrations measured in a number of different field campaigns in the Arctic (Creamean et al., 2022; Geerts et al., 2022; Hartmann et al., 2020, 2021; Li et al., 2023; Prenni et al., 2007; Porter et al., 2022; Rogers et al., 2001; Rinaldi et al., 2021; Sanchez-Marroquin et al., 2020, 2023; Wex et al., 2019). These are compared to mid-latitude INP measurements from precipitation samples collated by Petters and Wright (2015).

the INP measurements in ACAO, the two were consistent if the ACAO spectra were extrapolated log-linearly as the gradient of INP spectra in ACAO was lower than that measured by Li et al. (2023).

Comparison with the INP literature presents a somewhat confusing picture. It may simply be the case that there is strong variability in a range of spatial and temporal scales. However, there may also be differences between techniques. As noted in the methods section, intercomparison of assay techniques reveals similar results for some INP types (DeMott et al., 2018; Wex et al., 2019) but substantial differences between different techniques for some INP types (Hiranuma et al., 2019). Additionally, intercomparison of assay techniques on simultaneously taken samples of ambient aerosol during field campaigns has shown both consistencies and inconsistencies between techniques (Li et al., 2023; Lacher et al., 2024). Beall et al. (2020) report that biological INPs can sometimes be lost during storage and transport, which we largely avoid by processing our filters during the campaign in a temporary laboratory. While the droplet-on-filter technique used here was not included in the formal intercomparisons, it has shown different responses in other environments, and the results are consistent with what might be expected. For example, this technique produced INP concentrations several orders of magnitude smaller than in ACAO during March 2018 near Alaska (Sanchez-Marroquin et al., 2023). In dust plumes emerging from Africa, this technique produced much steeper INP spectra than in ACAO (Price et al., 2018), and the INP concentrations were consistent with laboratory-derived activity of K-feldspar in mineral dust (Harrison et al., 2019). Measurements in the UK revealed a strong biological "hump" consistent with ground-based measurements (Sanchez-Marroquin et al., 2021). In addition, measurements in dust plumes emerging from Iceland produced active site densities consistent with laboratory measurements of Icelandic dust (Sanchez-Marroquin et al., 2020) and other high-latitude dusts (Barr et al., 2023). Continued efforts are needed to intercompare INP assay techniques and better understand the influence of storage, but high Arctic INP concentrations have been observed by various groups using various techniques.

Overall, the literature in combination with our new measurements indicates that INP concentrations during northerly CAOs in this region, where the air is drawn from the central Arctic, can at least sometimes have mid-latitude-like INP concentrations.

3.2 Aerosol environment in CAOs

To try to understand the sources and variation in the high INP concentrations observed during the campaign, we used observations from the PCASP and CDP underwing probes to investigate the aerosol environments during filter sampling.

Size distributions of the aerosol particle number, N; surface area, S; and volume, V, are presented in Fig. 5. To derive surface area and volume, aerosols were assumed to be spherical. The size distributions of aerosol measured during the campaign were mostly similar in shape but with values of $\mathrm{d}N/\mathrm{d}\log(D)$ that spanned 2 orders of magnitude. Number concentrations of aerosol were dominated by submicron particles. Few super-coarse aerosol particles (diameter $D > 10\,\mu\mathrm{m}$) were observed, though particles with diameters greater than 30 µm were at the edge of the detection ability of the CDP. Sub- and supermicron particles contributed approximately equally to the total surface area of the aerosol. Number concentrations of aerosol observed were consistent with those observed over the Norwegian Sea during the March–April 2013 Aerosol-Cloud Coupling and Climate Interactions in the Arctic (ACCACIA) aircraft campaign using the PCASP and CDP instruments by Young et al. (2016). However, the number concentration of submicron aerosol was up to 2 orders of magnitude greater than in March observations of aerosol made near Ny-Ålesund by Song et al. (2021) from 2015–2019 using a ground-based aerodynamic particle sizer. The number concentration of aerosol with a diameter between 0.1–0.5 µm observed during ACAO was also an order of magnitude greater than that measured at Ny-Ålesund during the COMBLE campaign, though concentrations were similar between 0.5–1 µm (Williams et al., 2024).

Figure 6 shows aerosol profiles from each of the flights where PCASP and CDP data were available. Measurements of aerosol concentration where filter samples were taken are highlighted according to their INP concentration, showing that the INP filter samples taken were subject to aerosol concentrations representative of the aerosol environment at these heights measured throughout the flight. Aerosol concentrations near the sea surface (< 500 m a.s.l.) were consistently 100–200 cm^{-3}. These measurements were comparable to measurements made in early April 2022 near Svalbard during the HALO-$(\mathrm{AC})^3$ campaign (Wendisch et al., 2024). However, the vertical distribution of aerosol varied much more between flight days. On 3 flying days, aerosol concentrations were approximately constant from the surface up to 7500 m. These were c274, which had a northwesterly flow, and c277–c278 and c281–c282, which both had northerly flows. These contrasted with 3 d where the aerosol concentration decreased with altitude in the boundary layer. These were c273, which had a westerly flow, and c275–c276 and c279, which both had northerly flows. Finally, aerosol concentrations increased with altitude during flight c280, another day with a northerly flow.

3.3 Size-resolved aerosol composition

SEM analysis to determine size-resolved composition was performed on two polycarbonate filters sampled during filter runs c279r1 and c278r2. These filters were selected to represent the aerosol upstream of the CAOs and had an $N_{\mathrm{INP}}(-15\,^{\circ}\mathrm{C})$ of $(0.49 \pm 0.15)\,\mathrm{L}^{-1}$ and $(1.4 \pm 0.4)\,\mathrm{L}^{-1}$ respectively. These represent INP concentrations at the 33rd

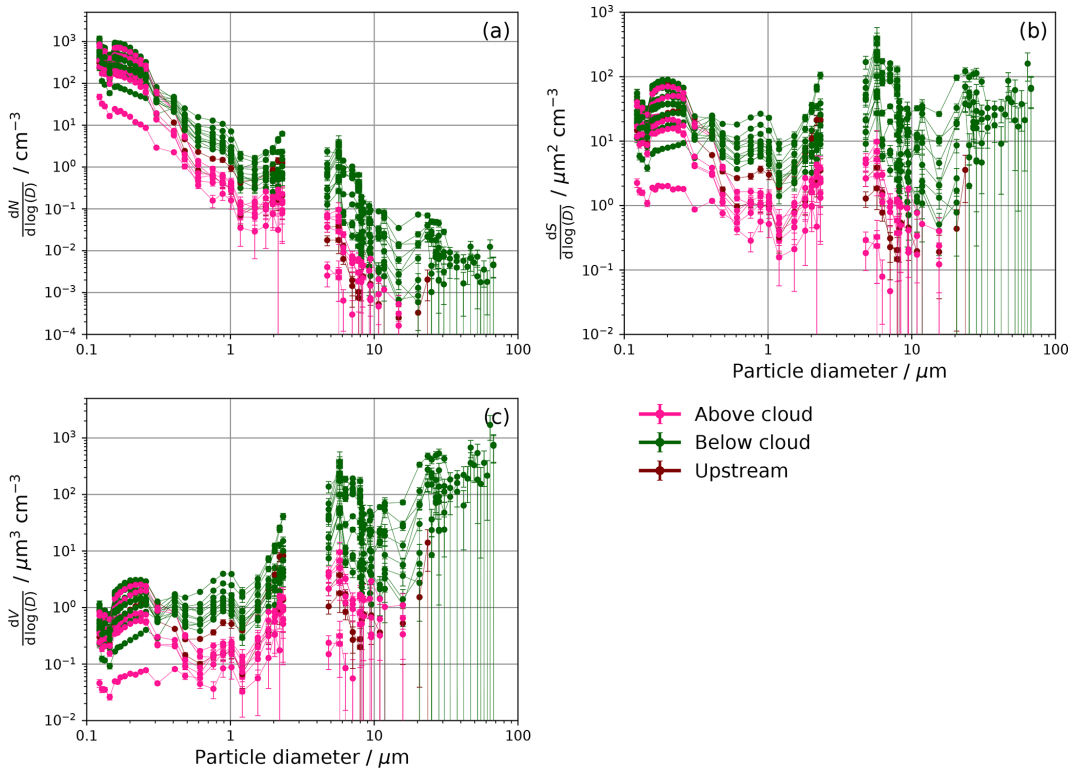

Figure 5. Size distributions of **(a)** particle number, **(b)** particle surface area and **(c)** particle volume measured with the PCASP and CDP probes during each filter sample. Probe data were unavailable during flights c271 and c272. A version of this figure where each size distribution is individually labelled according to the sample it is associated with can be found in Appendix A.

and 90th percentiles of samples taken in CAOs. Filter c279r1 was sampled at an altitude of 155 m over the marginal sea-ice zone, while filter c278r2 was sampled at an altitude of 1725 m above the Svalbard archipelago and surrounding sea ice, prior to cloud development. The size and elemental proportions of 1101 and 451 particles respectively were analysed on these filters.

Composition analysis and particle size distributions derived using SEM for each of the filters are shown in Fig. 7. Figure 7 also compares the particle size distributions derived using SEM with those derived from the PCASP and CDP. Both filters showed that a large proportion of the particles were consistent with mineral dusts, with Si-rich and Al- and Si-rich particles representing over half of the proportion of supermicron particles. There were also significant numbers of carbonaceous aerosol in the submicron range, although this method cannot confirm if they were of biological origin. We did not note any particles that were qualitatively of biological origin on the basis of size or morphology, as noted previously in Sanchez-Marroquin et al. (2021). However, due to the relatively small fraction of filter analysed, their presence cannot be ruled out. Despite filter sample c279r1 being taken close to the marginal ice surface, less than a quarter of the particles showed clear signatures of sea spray (such as the presence of both sodium and chlorine), though some of the carbonaceous or sulfurous aerosol could be of marine origin. The total surface area of mineral dust particles, being the sum of Si-rich, Si- and Al-rich, Si-only, and Ca-rich classes, was calculated as 1.0 and 0.6 $\mu m^2\,cm^{-3}$ for c279r1 and c278r2 respectively. These values are consistent with measurements of aerosols 91–375 m over the Norwegian Sea in March, made by Young et al. (2016) during the ACCACIA campaign. Filter c279r1 showed very few particles with clear sea-spray signatures, consistent with its higher altitude and location over sea ice. Metal-rich particles are present in the smaller-size fraction, although these have previously been found to be contaminant particles on blank filters. These were likely produced by the microscope mechanism, so it is not clear if they are artefacts or from the atmosphere.

The aerosol number measured by the SEM is generally 2–4 times below the aerosol number reported by the PCASP and CDP probes or shifted to about 30 % smaller sizes. Previous studies using this technique have also found similar magnitudes of discrepancy between the techniques. In these cases, SEM has sometimes measured more particles than the optical probes and sometimes less (Sanchez-Marroquin et al., 2020, 2021). Using a different SEM technique, Young et al. (2016) found the PCASP and CDP probes reported concentrations up to 100 times greater than SEM and attributed this larger discrepancy to measurements of cloud droplets

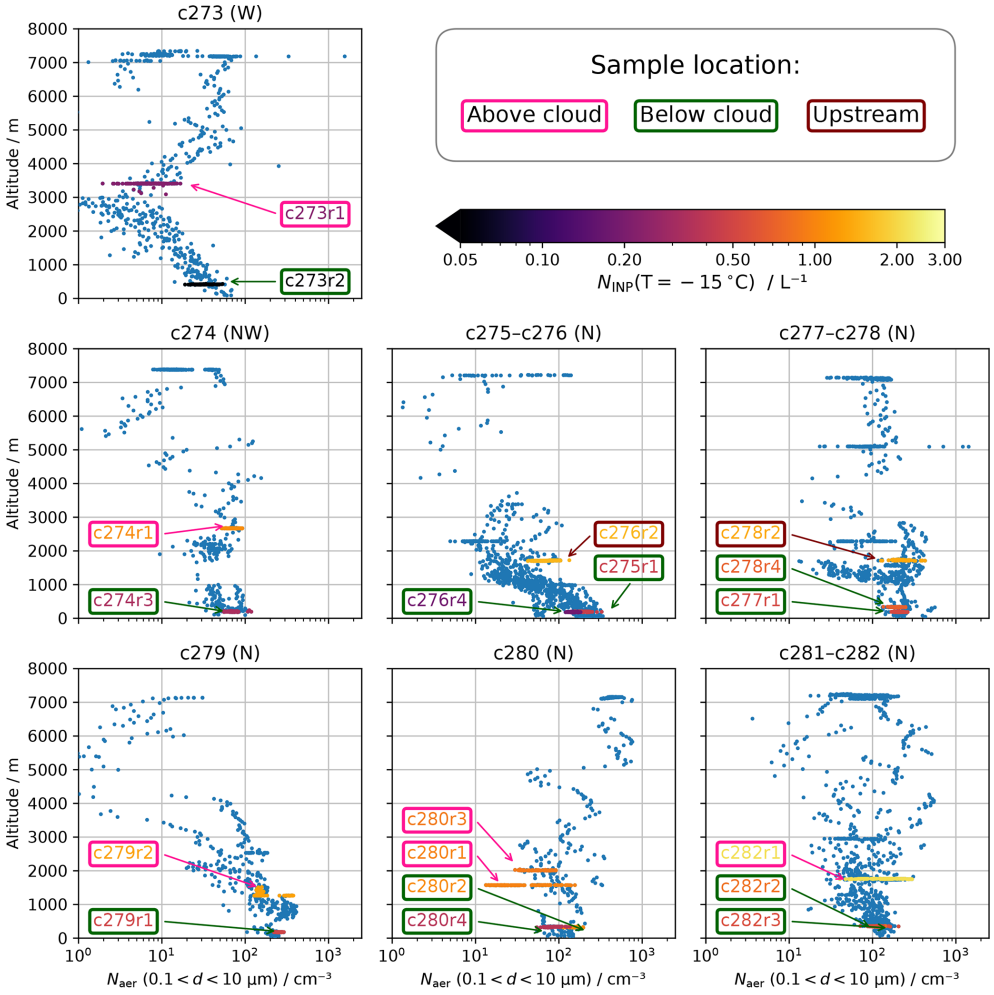

Figure 6. Out-of-cloud aerosol measurements made using the PCASP and CDP averaged every 10 s. Measurements made during filter sampling are coloured and labelled according to their INP concentration at $T = -15$ °C. The borders of each label and the arrows matching labels to measurements are coloured according to the location of the sample relative to the CAO cloud. Measurements over or close to the Scandinavian Peninsula were discarded to represent Arctic and oceanic air only.

or swollen aerosol since they sampled at high relative humidity (RH), often with RH > 90 %. We discarded PCASP measurements made in cloud or above RH = 80 % to bias against swollen aerosol. However, even at RH = 80 %, the diameter growth factor of typical organic aerosol has been reported to be between 20 %–50 % (Martin et al., 2003; Latimer and Martin, 2019). For sea salt, the diameter growth factor at RH = 80 % has been reported to be between 60 %–100 % (Tang et al., 1997; Martin et al., 2003; Murray et al., 2012a). Hygroscopic growth of these species might help explain our discrepancy. However, the measured size and number of the mineral dust particles should not be affected by humidity.

3.4 Ice-nucleating activity of samples

To determine how ice-nucleating activity depends on the physical properties of the aerosols, the aerosol size distributions presented in Fig. 5 were used to calculate the total aerosol number N_{aer}, surface area S_{aer} and volume V_{aer} for aerosols with $D > 0.1$ µm, assuming spherical geometry. Figure 3 shows the INP concentrations normalised by aerosol number, area and volume. Normalising N_{INP} by N_{aer} failed to reduce the spread in values between measurements, while normalising by S_{aer} and V_{aer} increased the spread between measurements. This indicates that the INP concentration does not scale with the overall aerosol surface area or volume. This is consistent with the INP being a subset of the aerosol particle population, with non-ice-nucleating components of the aerosol particle population being the primary driver of variability in S_{aer} and V_{aer}. Other studies of Arctic and high-latitude INPs (e.g. Porter et al., 2022; Barr et al.,

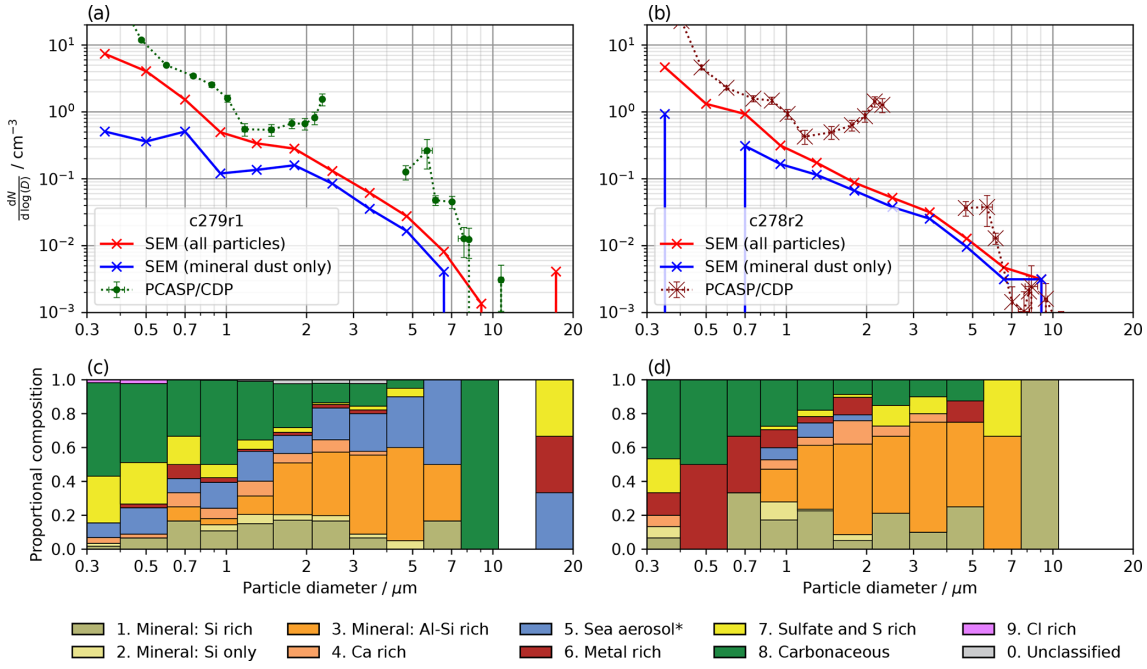

Figure 7. Particle size distributions and particle composition derived from scanning electron microscopy for filters c279r1 **(a, c)** and c278r2 **(b, d)**. Sample c278r2 was taken upstream of cloud development, while sample c279r1 was taken below the northern extent of CAO cloud streets. Both were taken in northerly CAOs. The solid lines show particle size distributions derived directly from the SEM measurements, while the dotted lines show the particle size distribution derived from the underwing probes in the diameter ranges, as in Fig. 5. Composition is shown for each size bin. Size bins with greater values of $\mathrm{d}N/\mathrm{d}\log(D)$ contain more particles. The white regions of the composition plots indicate that no particles were detected in this size range. Sea aerosol refers to aerosols likely to correspond to fresh, aged or mixed sea-spray aerosols.

2023; Sanchez-Marroquin et al., 2023; Moore et al., 2024) have also found that normalising by surface area fails to reduce the measurement spread.

In Fig. 8, measurements of $N_{\mathrm{INP}}/S_{\mathrm{aer}}$ are compared to measurements of active site density reported for well-defined samples and from other field campaigns. Both the magnitude and the shape of the curve of $N_{\mathrm{INP}}/S_{\mathrm{aer}}$ values from ACAO are similar to those measured by Porter et al. (2022) at the North Pole in late summer. This indicates that there is perhaps some commonality in INPs between these two campaigns, even though the timing and location were very different.

To compare $N_{\mathrm{INP}}/S_{\mathrm{aer}}$ to the active site density for well-defined samples, such as mineral dusts or sea spray, we note that these comprise only a fraction of the surface area in the aerosol samples in ACAO (see Fig. 7). In the case of sea spray, our $N_{\mathrm{INP}}/S_{\mathrm{aer}}$ values are many orders of magnitude greater than the active site density for pristine sea spray reported by McCluskey et al. (2018b); hence we conclude that the INPs we observe are not related to pristine sea spray.

Integration of the size distributions in Fig. 7 reveals that 32 % (c279p1) and 53 % (c278p2) of the overall aerosol surface area was mineral dust. Assuming that the aerosol composition was similar across the campaign, values of $N_{\mathrm{INP}}/S_{\mathrm{aer}}$ would be 2–3 times smaller than values of active site density normalised to the mineral dust surface area rather than the overall aerosol surface area. This allows us to compare with literature parameterisations of active site density for K-feldspar, desert dusts and soil dusts containing ice-active organic material in Fig. 8. Comparison with K-feldspar, the most active mineral component of atmospheric mineral dusts (Harrison et al., 2019; Vergara-Temprado et al., 2017), shows that K-feldspar alone cannot account for the magnitude of the observed active site densities above −20 °C as the temperature dependence is too steep. This implies that there is some other component in these samples that nucleates ice. Above −20 °C, measurements fall between the active site densities reported for agricultural soil by Steinke et al. (2016), fertile soils by O'Sullivan et al. (2018) and general mineral dusts (from fertile and infertile sources) by Niemand et al. (2012). The measurements are also similar to the active site densities for supermicron Asian dust reported by Chen et al. (2021) and Icelandic dust measured by Sanchez-Marroquin et al. (2020).

In conclusion, the high values of $N_{\mathrm{INP}}/S_{\mathrm{aer}}$ of the ACAO samples at temperatures greater than −20 °C suggest a strong biogenic component to the INP population (Huang et al., 2021), potentially corresponding to mineral dust containing biological components, such as fertile soils.

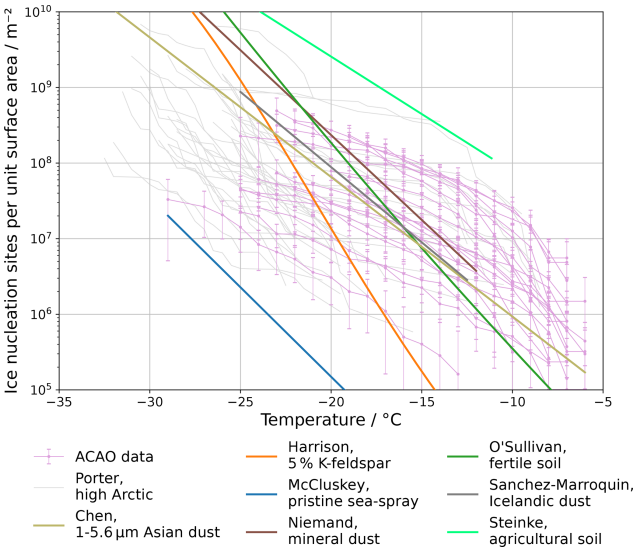

Figure 8. A comparison of N_{INP}/S_{aer} measured during the ACAO campaign to measurements of active ice nucleation site density in the high Arctic by Porter et al. (2022) and parameterisations of active ice nucleation site density (Chen et al., 2021; Harrison et al., 2019; McCluskey et al., 2018b; Niemand et al., 2012; O'Sullivan et al., 2018; Sanchez-Marroquin et al., 2020; Steinke et al., 2016).

3.5 Variation in INP properties with altitude and position in CAOs

To understand how the INP spectra varied with altitude during ACAO, we considered the variation of INP properties with altitude in northerly CAOs (flights c274 to c282). In Fig. 9, INP concentrations at −15 °C ($N_{INP}(-15\,°C)$), as well as the same quantity normalised by surface area, are presented relative to the altitude of the samples. This temperature was chosen to be representative of typical cloud temperatures in ACAO and because spectra with relatively high INP concentrations at −15 °C had similarly high concentrations relative to other INP spectra in the campaign across all temperatures.

Considering $N_{INP}(-15\,°C)$, the samples fall into two groups, as shown in Fig. 3. Samples taken above the clouds and upstream of the clouds fall into a group where mean $N_{INP}(-15\,°C) = 1.3\,L^{-1}$ above the cloud, whereas the below-cloud value is $0.54\,L^{-1}$. This indicates that the below-cloud INP concentrations are approximately 2.4 times smaller than the above-cloud measurements. This is consistent with a free tropospheric source of INPs rather than a source from the surface. It is also possible that there is a removal of INPs in clouds, which we return to below. When normalised to the aerosol surface area ($N_{INP}(-15\,°C)/S_{aer}$), the gap between the two groups is even larger, with above-cloud values approximately 8.8 times larger than the below-cloud values. Similar relationships between INP activity and altitude were found by Moore et al. (2024), who observed that INP concentrations normalised by surface area above the cloud in the SOCRATES campaign were greater than those below the cloud. Additionally, Knopf et al. (2023) found that during measurements on INPs in the eastern North Atlantic, the efficiency of deposition ice nucleation was greater for samples taken in the free troposphere than in the marine boundary layer. The reduced $N_{INP}(-15\,°C)/S_{aer}$ below the cloud is due to the enhanced aerosol surface area below the cloud in the CAO that was most likely related to the enhanced sea-spray production (consistent with the visual observations of extreme sea states related to the high wind speeds in the CAOs that we flew in). The enhanced aerosol surface area below the cloud compared to above the cloud is clear from Fig. 5. This reduction in activity is consistent with the sea spray producing a negligible concentration of INPs (see Sect. 3.4) and so contributing additional aerosol surface area with limited ice-nucleating ability. Using the average below-cloud aerosol surface area with the parameterisation of McCluskey et al. (2018b), the INP concentration at −15 °C would be expected to be $4 \times 10^{-4}\,L^{-1}$ if the only INPs below the cloud were sea spray. Our measured INP concentration is more than 3 orders of magnitude greater than this, again indicating that sea spray is not an important INP type in these CAO events.

On three flights (Table 2), two below-cloud filter samples were taken at different points in the CAO. We might expect aerosol and INP scavenging to increase further south as CAOs develop, especially in the cumulus regime where intense precipitation might efficiently remove particles. A downwind decrease in aerosol number concentration in Norwegian Sea CAOs attributed to precipitation scavenging has previously been observed by Williams et al. (2024). Using the values of $N_{INP}(-15\,°C)$ and the total aerosol surface area S_{aer}, we calculated the factors of change in INP concentration (F_{INP}), ice-nucleating activity (F_S) and surface area (F_{aer}) between the upwind and downwind measurements:

$$F_{INP} = \frac{N_{INP}(-15\,°C,\ \text{downwind})}{N_{INP}(-15\,°C,\ \text{upwind})},$$
$$F_S = \frac{N_{INP}(-15\,°C,\ \text{downwind})/S_{aer}\ (\text{downwind})}{N_{INP}(-15\,°C,\ \text{upwind})/S_{aer}\ (\text{upwind})},$$
$$F_{aer} = \frac{S_{aer}\,(\text{downwind})}{S_{aer}\,(\text{upwind})}. \quad (5)$$

These values are displayed in Table 2 with the difference in latitude between the measurements, $\Delta\varphi$. Both the INP concentration and the ice-nucleating activity decreased with latitude. The total surface area of the aerosol increased in two flights by 69 % and 85 % but decreased by 25 % in one pair. The upwind filters were sampled under stratocumulus conditions, while the downwind filters were in a mixture of stratocumulus and cumulus, with precipitation in two cases (c280r4 and c282r3).

During flight c280, two pairs of above- and below-cloud filter samples were taken along the same wind trajectory (Fig. 1b). The northern pair was taken where the clouds had

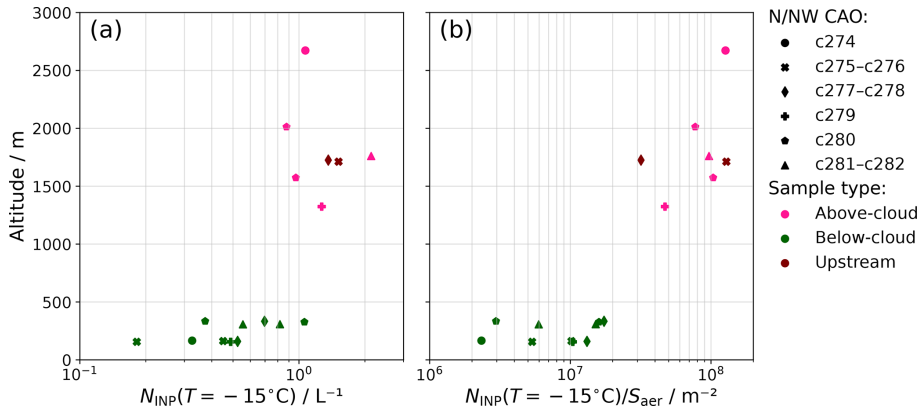

Figure 9. Variation with altitude of **(a)** INP concentration at −15 °C and **(b)** INP concentration at −15 °C normalised by aerosol surface area in northerly CAOs.

Table 2. Factors of change in the INP concentration at −15 °C (F_{INP}), INP concentration normalised by surface area at −15 °C (F_S) and total aerosol surface area (F_{aer}) between three pairs of below-cloud filter measurements.

Flight	Upwind filter	Downwind filter	$\Delta\varphi$	F_{INP}	F_S	F_{aer}
c275–276	c275r1, Sc	c276r4t, Sc	1.92	0.40	0.52	0.75
c280	c280r2, Sc	c280r4t, precipitating Cu	2.17	0.35	0.19	1.85
c281-282	c282r2, Sc	c282r3t, precipitating Sc–Cu	3.58	0.68	0.39	1.69

stratocumulus forms, whereas the southern pair was taken where the clouds were in the cumulus regime. Comparing the INP spectra for these samples in Fig. 10 shows that except at the very highest temperatures, where the error is large, there is little difference between the samples taken above and below the stratocumulus (c280r1 and c280r2 respectively) and the sample taken above the cumulus (c280r3). Closeness between the three INP measurements may be expected if the main INP source entering the system is upwind of the CAO clouds. However, the southern sample taken below the cumulus (c280r4) has over 5 times fewer INPs at temperatures below −11 °C.

Together, these results are consistent with INPs being removed by cloud and precipitation scavenging in the CAO, although this conclusion is based on only three cases. If precipitation scavenging is strong, it is possible that the INP concentrations measured during ACAO could be consistent with the INP concentrations measured at Andenes by Geerts et al. (2022). As such, it would be helpful to test this with future aircraft INP measurements much deeper into the cumulus regime (i.e. further south). This was not feasible in ACAO due to a combination of unfavourable meteorology, airspace restrictions and the prioritisation of tasks within the available flight time.

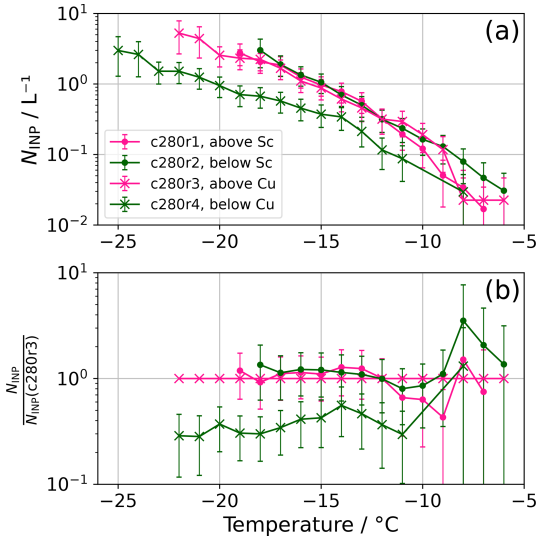

Figure 10. Panel **(a)** shows the four filter samples taken during flight c280 and describes their location relative to either stratocumulus (Sc) or cumulus (Cu) clouds. Panel **(b)** shows their INP concentrations relative to c280r3 (the sample taken above the cumulus) for the temperature ranges over which they can be compared.

3.6 Backward-trajectory analysis

To investigate the potential sources of sampled aerosol, backward trajectories were produced for each sample using

the Hybrid Single-Particle Lagrangian Integrated Trajectory (HYSPLIT) model (Stein et al., 2015). Meteorological data from the Global Data Assimilation System (GDAS) at 1° resolution were used to obtain the trajectories. The backward trajectories were run for 7 d and initiated along each flight track at 3 min intervals during each of the sampling periods to produce multiple trajectories. Figure 11a shows these trajectories, and Fig. 11b shows the INP concentration at $T = -15\,°C$ associated with each air mass. The majority of the air masses associated with northerly cold-air outbreaks circulated in the high Arctic for several days. Air masses associated with westerly CAOs (c273, c274) typically passed over Greenland, the Atlantic Ocean or Canada. Some of the air masses associated with northerly CAOs passed over Asiatic mid-latitudes 6–7 d prior to sampling. However, there was no clear correlation between INP concentration and air mass origin, suggesting that the air masses did not interact with a distinct source of INPs in 7 d transport. This might be consistent with a diffuse INP source across the whole of the Arctic region or INPs that were emitted further back in time than 7 d ago and transported into the Arctic where they circulated around in the Arctic's stable atmosphere prior to being drawn out in CAO events. We return to these ideas in the next section.

4 Discussion of potential INP sources

The INP concentrations measured during the ACAO campaign were amongst some of the highest measured in the Arctic (Fig. 3 and associated discussion). We now discuss several possible explanations for these high concentrations and thus the potential sources of INPs.

If the INPs were of local origin, strong local sources of INPs would be required to explain the high INP concentrations. Potential local sources of INPs in the region of the Norwegian Sea (Fig. 1a) include upstream INP sources from Arctic land such as the Svalbard archipelago; continental INPs from Europe; and sea-spray aerosol from the open sea, polynyas and open leads. However, there are several reasons why these Arctic sources are unlikely to play a major role.

The presence of dust indicated by the SEM analysis and the consistency of the measured active site densities shown in Fig. 8 with those previously measured for biologically enhanced mineral dusts could indicate a local terrestrial source of INPs. It has been shown that mineral dusts from high-latitude sources contain ice-active biogenic materials (Barr et al., 2023; Tobo et al., 2019; Xi et al., 2022); hence dust might be sourced from the Svalbard archipelago or Greenland. However, back-trajectory analysis does not indicate that air masses directly from Svalbard or Greenland are consistently associated with the most active INP samples. Additionally, the pristine snow cover over land in March means that emissions of aerosol are strongly suppressed and are therefore unlikely to dominate the INP population observed during ACAO (Bullard et al., 2016; Meinander et al., 2022). Although there have been reports of dust emission events in Svalbard happening as early in the year as May (Dörnbrack et al., 2010), these events in Svalbard are typically reported in autumn when snow cover is at its minimum (Meinander et al., 2022; Rymer et al., 2022).

It is also unlikely that transport of mid-latitude continental INPs from Europe directly into the cold-air outbreak regimes was a dominant source of INPs since the cold-air outbreak conditions exhibited northerly or westerly flows. Early in the campaign, prolonged warm-air intrusion conditions exhibited southwesterly winds. However, some of the INP concentrations measured in the cold-air outbreak immediately after the warm-air intrusion had subsided (c273r2) were the lowest measured in the campaign.

Several aspects of the measurements suggest that sea-spray aerosol from the open sea was neither the dominant INP source nor a significant contributor to the ice-nucleating activity. Neither of the aerosol samples analysed with SEM showed that aerosols with clear sea-spray origins dominated the aerosol number, with less than 20 % of the aerosol in the sample taken at an altitude of 155 m over the marginal ice zone having a sea-spray origin. In the boundary layer, the measured INP concentrations were several orders of magnitude higher than those measured in similarly remote areas in the Southern Ocean or the North Atlantic where sea-spray aerosol is the dominant INP source (McCluskey et al., 2018a, b; Schmale et al., 2019; McFarquhar et al., 2021; Tatzelt et al., 2022). Furthermore, while the INP concentrations were similar above and below the cloud decks, the samples with the highest active site density were found above the cloud systems and in particular upstream of the outbreak (Fig. 9), environments unlikely to have large sea-spray components. Considering all these aspects, it is unlikely that sea-spray aerosol was a dominant source of INPs.

A final potential local source of INPs is the sea ice and leads in the sea ice. It has previously been hypothesised that open leads could be a significant source of INPs in the Arctic (Bigg and Leck, 2001). However, observed INP concentrations from ship campaigns passing through leads have found INP concentrations several orders of magnitude below those measured in ACAO (Bigg and Leck, 2001; Creamean et al., 2022). Furthermore, backward trajectories from the high Arctic measurements of INPs by Porter et al. (2022) showed that air masses which had spent the majority of the past week over sea ice had the lowest INP concentrations. Snow blown from the surface of sea ice has been shown to be a source of sea salt aerosol (Yang et al., 2008; Gong et al., 2023), though there has been little investigation into this mechanism as a potential INP source, and the reduced activity of INP samples below the cloud deck again suggests that this would be unlikely to dominate the INP population. Together, these suggest that sea ice was not a dominant source of INPs during the ACAO campaign.

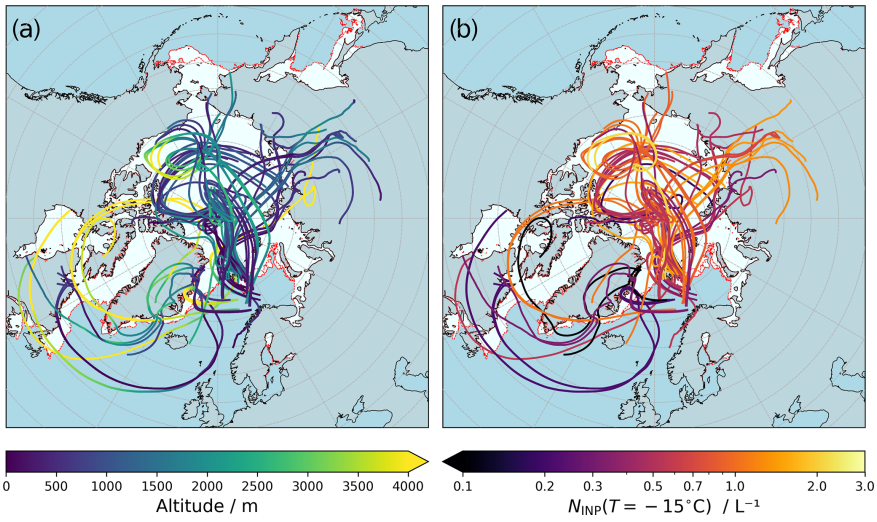

Figure 11. The 7 d backward trajectories of air masses sampled. Two trajectories are shown for each sample, corresponding to the start and end of the sampling periods. There was little variation in trajectories at intervals within the sampling periods. Panel **(a)** shows the altitudes associated with the trajectories, while panel **(b)** shows the relative magnitude of INP concentration, ν_{INP}. Backward trajectories from c272r6, measured in a warm-air intrusion, are not included.

Further evidence against a local surface source of INPs is that INP concentrations in northerly CAOs were fairly constant with altitude up to 3 km (Fig. 9). A local surface source would lead to enhanced INPs at the surface in the highly stable stratified atmosphere of the Arctic in winter and early spring. However, high INP concentrations are persistent during all flights between 21 and 30 March across a wide area. Additionally, there are no large-scale ascending air masses exiting the Arctic that would carry the aerosol to 3 km altitude, and convection is limited to altitudes lower than 2.5 km even in well-developed CAOs.

Since it is unlikely that the dominant INPs had a local terrestrial or marine source, it follows that the high INP concentrations are likely to have originated from long-range transport. During the boreal winter, aerosol in the Arctic atmosphere can then have lifetimes of the order of weeks or months as a result of the dry and stable conditions leading to weak aerosol scavenging (Carslaw, 2022). Coupled to this, we know that transport into the Arctic over the winter months leads to the build up of pollution, predominantly from Eurasian sources, which gives rise to the phenomenon of Arctic haze (Shaw, 1995; Stohl, 2006; Ekman and Schmale, 2022). While the anthropogenic component of Arctic haze has received substantial attention, it is also well known that other mid- and low-latitude aerosols are transported into the Arctic along with this pollution aerosol, such as mineral dust from African and Asian deserts (Rahn et al., 1977; Shi et al., 2022). Barrie (1986) suggested that the Arctic front extends as far south as 40° N in winter over the Eurasian landmass, encompassing sources such as Asian deserts and numerous pollution sources. Arctic haze layers have been reported to occur up to approximately 9 km altitude and have spacial extents of the order of 1000 km (Barrie, 1986). Our measurements of a widespread and vertically uniform distribution of INPs exiting the Arctic during the second half of March 2022 are consistent with a vertically extensive "reservoir" of INPs in the Arctic that is similar to pollution-related haze.

Previous airborne measurements of Arctic haze by Borys (1989) have suggested that Arctic haze, when identified by large signatures of anthropogenic pollutants, had 10–100 times fewer active INPs at −25 °C than Arctic aerosol samples with fewer pollutants. However, these low-pollutant samples may have been transported into the Arctic from low-latitude INP-rich environments, like desert regions, without being mixed with anthropogenic sources. Accordingly, aerosol traditionally defined as Arctic haze due to its large pollution signature may not be associated with aerosol of lower-latitude origins that has a high INP content. Springtime measurements of dust over the Norwegian Sea by Young et al. (2016) during the ACCACIA field campaign were attributed to long-range transport and had elemental composition ratios similar to those from Asian dust. During the ACCACIA campaign, plumes of aerosol from eastern and northern Asia were observed, which were hypothesised to have transported dust to the region (Liu et al., 2015; Young et al., 2016). As mentioned above, Asian dust has been thought to be a source of Arctic haze since the 1970s (Rahn et al., 1977), while recent modelling by Shi et al. (2022) has shown that during the spring months, less than 20 % of the Arctic dust load above 900 hPa was emitted into the Arctic and that approximately 50 % of the dust load at all heights came from Asia. Modelling by Groot Zwaaftink et al. (2016) also attributed approximately 38 % of the Arctic dust load to Asian

sources. This is significant since Asian dust is known to contain ice-active biological components (Creamean et al., 2013; Chen et al., 2021), which might be consistent with high ice-nucleating activities akin to those observed in ACAO. Transport routes for such biogenic-containing Asian dust have been demonstrated by Zhao et al. (2022), while year-round lidar observations by Ansmann et al. (2023) in the high Arctic have suggested that a small fraction of dust aerosols may control ice nucleation outside of summer. Based on the above evidence, we suggest that the dominant INP observed in ACAO was mineral dust internally mixed with ice-nucleating biogenic materials that originated from the lower latitudes and was transported into the Arctic through similar transport routes to Arctic haze.

The hypothesis of an INP reservoir appears to contradict previous remote sensing studies that used observations of Arctic clouds to infer spatial variations in INP concentrations. For instance, Carlsen and David (2022) define a temperature, T^*, at which mixed-phase clouds become more frequent than liquid clouds and use this as a proxy for freezing initiated by INPs. They find that in winter, when Arctic haze builds up, T^* is lower over the sea ice than over the open sea, which they attributed to a suppression of INP emissions (and concentrations) caused by sea-ice cover. However, differences in ice concentrations between ice-covered and ice-free regions in high Arctic clouds may not reflect differences in INP concentration but rather differences in cloud microphysics related to cloud dynamics. For example, clouds over ice are shallow, long-lived and relatively stable compared to the deeper clouds with colder tops over ocean regions (Morrison et al., 2012; Arteaga et al., 2024). The long lifetime of these Arctic clouds provides time for INPs to be scavenged from the atmosphere; thus their small ice content may be a consequence of their history rather than the INP concentration when they first formed. Similarly, Murray-Watson and Gryspeerdt (2024) used satellite observations to suggest that increasing ice concentrations downwind in CAOs imply increased INP concentrations downwind, associating this with increased emissions of sea-spray INPs. This contrasts with our linked in situ measurements of below-cloud INPs that reveal a decrease in INP concentration downwind (Table 2). The increased downwind ice concentrations observed by Murray-Watson and Gryspeerdt (2024) may be related to secondary ice processes, rather than INPs, since these are associated with strongly convective clouds, which are more likely to occur downwind. Additionally, clouds later in the CAOs tend to have lower cloud-top temperatures, naturally increasing the concentrations of ice.

5 Summary and conclusions

We made the first airborne measurements of INPs targeted at cold-air outbreaks over the Norwegian and Barents seas. We took 23 filter measurements and performed droplet-freezing assays using a droplet-on-filter technique to determine INP concentration. INP concentrations measured over a large area of the Norwegian and Barents seas at altitudes between 40–3400 m were amongst the highest reported in the Arctic, with $N_{\mathrm{INP}}(-15\,^{\circ}\mathrm{C})$ ranging from 0.18–2.1 L^{-1} when the airflow had a strong northerly component. This indicates that high INP concentrations were horizontally and vertically widespread in these northerly flows, conducive to CAOs and boundary layer cloud formation, and persisted for at least 12 d in late March. These high INP concentrations contrast with previous surface measurements made in the same region and at the same time of the year but overlap with other airborne measurements using an online measurement technique. The lowest INP concentrations we measured during ACAO, $N_{\mathrm{INP}}(-15\,^{\circ}\mathrm{C}) = 0.03\,\mathrm{L}^{-1}$, were in a westerly CAO. These results, combined with the literature data, highlight the importance of targeting INP measurements during specific meteorological events since an average INP concentration for this region and time would probably not represent the INP population for specific CAO clouds well.

To investigate the source of the high INP concentrations, we used particle size data from the underwing probes of the aircraft to normalise the INP concentration by the total aerosol surface area to gain an estimate of the density of active ice nucleation sites across the samples. Comparing this to literature measurements of active site density suggested that the INP population was likely dominated by mineral dust with ice-active biogenic components. Additionally, the samples with the highest ice-active site densities were found above the cloud system, suggesting that the INP population was not dominated by sea-spray aerosol. Scanning electron microscopy with energy-dispersive X-ray spectroscopy on two filters collected upstream of the cold-air outbreaks showed that the presence of mineral dusts accounted for 30 % or more of the aerosol surface area. Considering the meteorology during the campaign and activity of the samples, it is likely that the majority of the INPs did not come from local sources but instead from long-range-transport mechanisms more commonly associated with the Arctic haze phenomenon. As such, we suggest that the high INP concentrations measured during the ACAO campaign were due to the presence of biogenically enhanced dust, which dominated the ice nucleation processes, rather than sea-spray aerosol, in spite of the remoteness of the region.

These new measurements of INP concentrations measured in the ACAO campaign raise important questions for our understanding of Arctic mixed-phase clouds. The strength of the cloud-phase feedback depends on the balance between ice and liquid in clouds in the present day, with clouds with more ice having a greater negative feedback on climate in a warming world (Murray et al., 2021). Our results suggest that the magnitude of the cloud-phase feedback may be larger in Northern Hemisphere CAOs compared to their Southern Ocean equivalents, where it has been shown that the INP populations are many orders of magnitude smaller than in

ACAO. Clearly, further work is needed to establish how representative ACAO was for CAO conditions in the Arctic. Nevertheless, future modelling work should investigate the response of Arctic mixed-phase clouds with these INP concentrations to warming to reduce the uncertainty in this feedback.

The high INP concentrations measured in ACAO may also impact the transition between stratocumulus and cumulus clouds in CAOs, which is partially controlled by precipitation (Abel et al., 2017). Since enhanced INP concentration can enhance ice growth and thus precipitation, these high INP concentrations may act as a control on CAO development. Modelling that investigates the strength of the control that INP concentration exhibits on CAO development will be useful for understanding the impact of INPs on CAO cloud cover and thus radiative forcing. Finally, airborne measurements above and below the cloud deck have helped to establish the dominant INPs in these case studies. We recommend that more aircraft measurements be made in air that is of direct relevance to clouds in order to better understand the relationship between cold-air outbreak cloud properties and INPs.

Appendix A: Individual INP spectra and associated aerosol size distributions

Figures A1 and A2 show individually labelled INP spectra and aerosol size distributions respectively, as in Figs. 3 and 5 where they are grouped by location relative to the cloud.

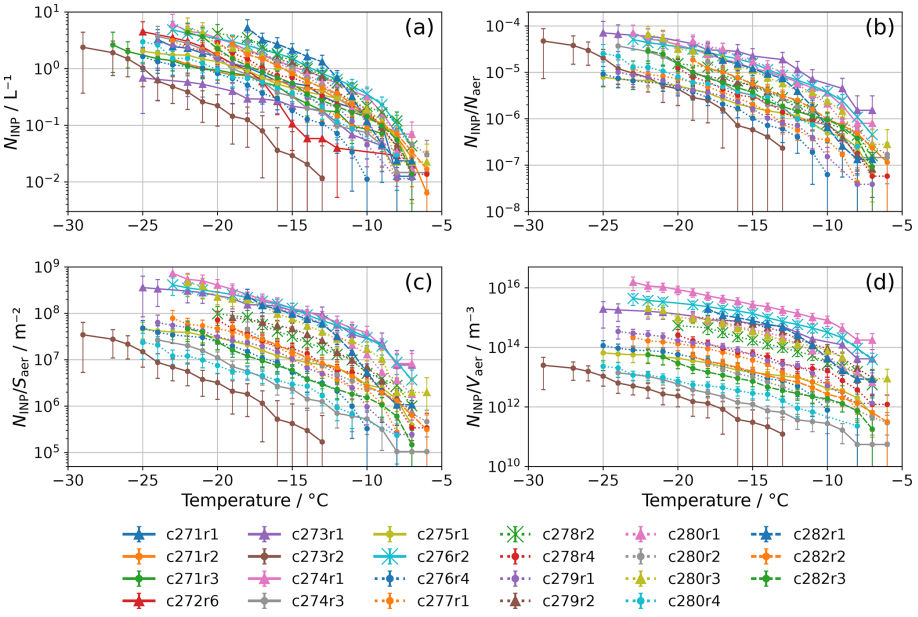

Figure A1. Panel **(a)** shows INP concentrations for each sample taken during the campaign. Panels **(b)**, **(c)** and **(d)** show these concentrations normalised by the total number (N_{aer}), surface area (S_{aer}) and volume (V_{aer}) of aerosols with diameters greater than 0.1 µm.

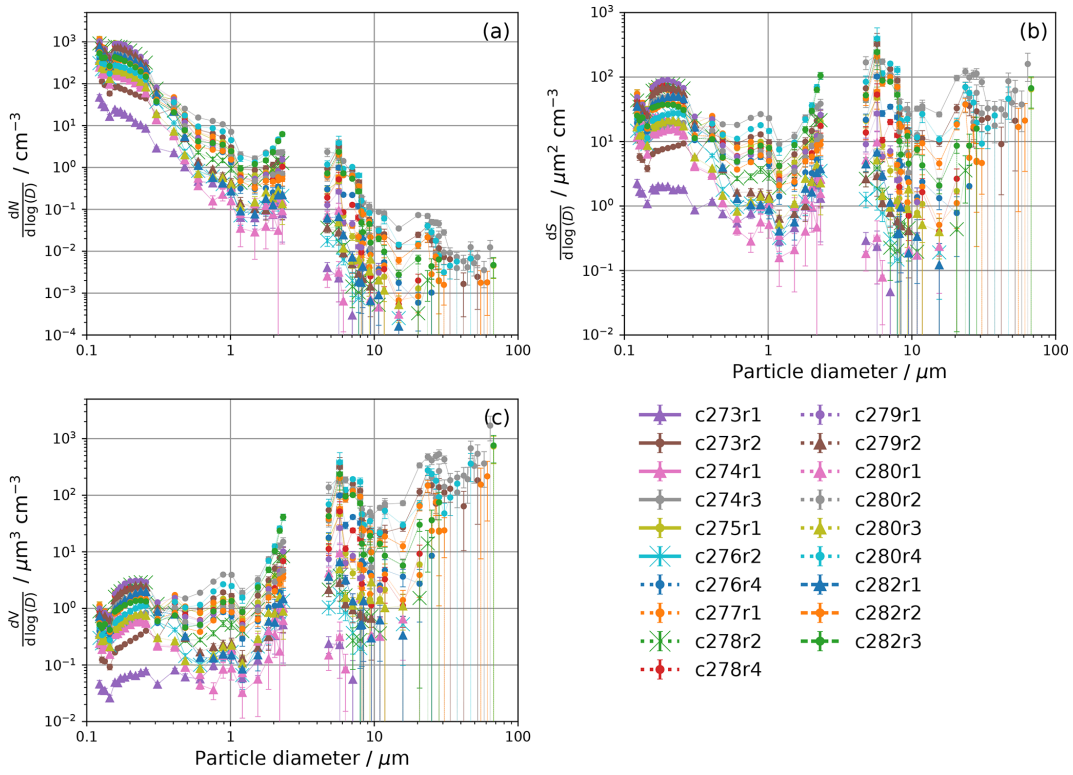

Figure A2. Size distributions of **(a)** particle number, **(b)** particle surface area and **(c)** particle volume measured with the PCASP and CDP probes during each filter sample. Probe data were unavailable during flights c271 and c272.

Appendix B: INP spectra curve fitting

Our measurements show that the entire INP spectrum ($N_{INP}(T)$) varied over the campaign (Fig. 3). To represent the INP concentration across the full temperature spectrum in future modelling work, particularly when modelling individual case studies, we fitted all spectra to a four-parameter function. This function took the form

$$N_{INP} = \nu_{INP} \exp\left[a(T_{max} - T)^b\right]. \quad \text{(B1)}$$

The parameter T_{max} represents the greatest temperature at which a freezing event was observed, a and b are shape parameters that determine the curvature of the function, and ν_{INP} is a scale parameter related to INP concentrations (if the shapes were constant). For INP spectra with the same shape, greater values of ν_{INP} indicate greater INP concentrations across the entire temperature range. The same functional form was also applied to active site density spectra, which were fitted to the equation

$$N_{INP}/S_{aer} = \nu_S \exp\left[a(T_{max} - T)^b\right]. \quad \text{(B2)}$$

Fitting parameters for all spectra are given in Table B1, while examples of this fitting are shown in Fig. B1, where functions for three individual samples, c273r2, c277r1 and c276r2, are illustrated. These represent filter measurements with low, medium and high INP concentrations and active site densities and demonstrate the ability of the function to represent all INP concentrations during the campaign. Equations (B1) and (B2) were also used to create parameterisations for the median INP concentration and active site density across the campaign for springtime CAOs in the region (excluding c272r6, which was not taken in cold-air outbreak conditions). These are also shown in Fig. B1.

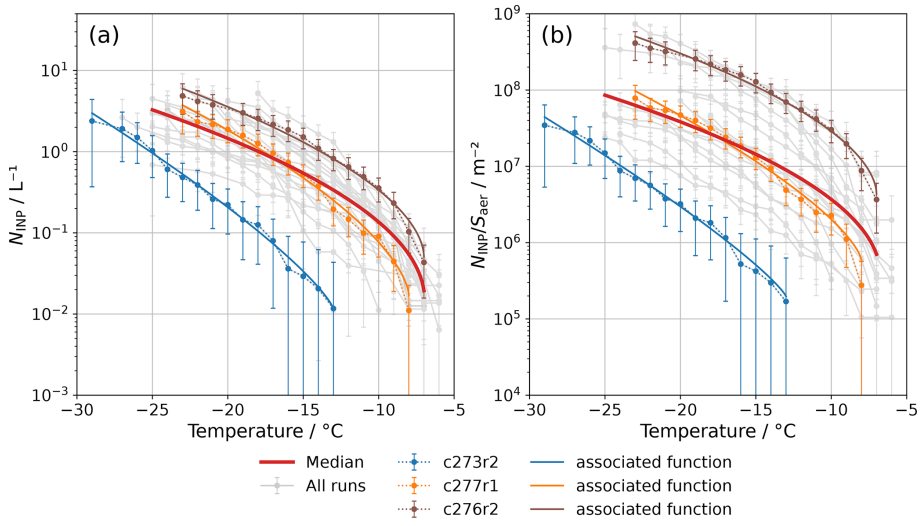

Figure B1. All measured temperature spectra for **(a)** INP concentration and **(b)** INP concentration normalised by aerosol surface area were fitted to Eqs. (B1) and (B2) respectively. In both panels, examples of fits to randomly chosen spectra with relatively high, medium and low INP spectra are demonstrated. In panel **(a)**, the red line shows the function fitted to the median INP concentration observed during the campaign, where $\nu_{INP} = 1.480 \times 10^{-2}\,L^{-1}$, $T_{max} = 266.2\,K$, $a = 1.271\,K^{-b}$ and $b = 0.5$. In panel **(b)**, the red line shows the function fitted to the median active site density observed during the campaign, where $\nu_S = 3.712 \times 10^{5}\,m^{-2}$, $T_{max} = 266.4\,K$, $a = 1.273\,K^{-b}$ and $b = 0.5$.

Table B1. Values of parameters that describe INP concentration (N_{INP}) and INP concentration normalised by surface area (N_{INP}/S_{aer}) using Eqs. (B1) and (B2) respectively. There is no parameterisation of N_{INP}/S_{aer} for flights c271 and c272 due to a lack of aerosol size data. Similar parameterisations for INP concentration normalised by N_{aer} and V_{aer}, not presented in this paper, can be found with other metadata at https://doi.org/10.5281/zenodo.11221599 (Raif et al., 2024).

	N_{INP}				N_{INP}/S_{aer}			
Sample ID	$\nu_{INP}(10^{-2}\,L^{-1})$	T_{max}(°C)	a	b	$\nu_S(10^6\,m^2)$	T_{max}(°C)	a	b
c271r1	2.524	−7.00	0.843	0.619	–	–	–	–
c271r2	1.964	−6.00	0.975	0.531	–	–	–	–
c271r3	1.760	−7.67	1.050	0.525	–	–	–	–
c272r6	0.492	−6.00	0.607	0.849	–	–	–	–
c273r1	1.087	−6.96	1.031	0.500	5.692	−6.96	1.031	0.500
c273r2	1.156	−13.00	0.616	0.793	0.197	−13.00	0.533	0.836
c274r1	3.368	−6.64	1.050	0.570	3.993	−6.64	1.050	0.570
c274r3	0.415	−4.00	0.606	0.818	0.193	−6.00	0.311	0.960
c275r1	2.484	−7.00	0.972	0.539	0.596	−7.00	0.933	0.548
c276r2	5.088	−7.00	1.029	0.553	4.346	−7.00	1.030	0.552
c276r4	1.557	−10.00	1.032	0.570	0.462	−10.00	1.031	0.570
c277r1	1.690	−8.00	0.978	0.631	0.587	−8.00	0.757	0.652
c278r2	4.343	−7.00	0.885	0.654	1.011	−7.00	0.960	0.652
c278r4	1.095	−5.97	1.050	0.619	0.273	−5.97	1.050	0.619
c279r1	1.108	−7.00	1.050	0.605	0.269	−7.00	0.960	0.629
c279r2	2.364	−7.00	1.003	0.640	0.832	−7.00	1.049	0.626
c280r1	1.556	−7.00	1.050	0.653	1.665	−7.00	1.050	0.653
c280r2	3.160	−6.00	0.474	0.903	0.477	−6.00	0.474	0.903
c280r3	1.320	−5.87	1.050	0.624	1.163	−5.87	1.050	0.624
c280r4	1.291	−7.44	1.050	0.563	0.163	−7.81	0.834	0.617
c282r1	2.188	−7.00	1.050	0.701	0.991	−7.00	1.050	0.701
c282r2	1.223	−5.87	1.050	0.630	0.226	−5.87	1.050	0.630
c282r3	3.707	−7.00	0.426	0.880	0.368	−7.00	0.472	0.847

Code and data availability. Code used for analysis and the creation of the figures in this paper can be found at https://doi.org/10.5281/zenodo.11221398 (Raif, 2024). Raw and processed INP data and metadata, processed aerosol size data and INP data normalised by N_{INP}/S_{aer}, HYSPLIT inputs and outputs, and Nevzorov clear-air flags can be found at https://doi.org/10.5281/zenodo.11221599 (Raif et al., 2024). Flight data from the FAAM aircraft are stored in the CEDA archive at https://catalogue.ceda.ac.uk/uuid/01021a90c0c2481c909bdb145cb72398 (Facility for Airborne and Atmospheric Measurements, 2024).

Author contributions. The work was conceptualised by ENR, KSC, BJM, PRF, SJA and SLB. Flights were planned by SJA, PAB, KNB, PRF, BJM and ENR. Experiments were carried out by SLB, MDT, JBM, BJM, MID and ENR. Formal analysis was carried out by ENR, while data were curated by ENR, MID and SJA. Python code was written by ENR and SLB. The original draft was written by ENR and reviewed by all authors. The work was supervised by KSC, BJM and PRF. Funding was acquired by BJM.

Competing interests. At least one of the (co-)authors is a member of the editorial board of *Atmospheric Chemistry and Physics*. The peer-review process was guided by an independent editor, and the authors also have no other competing interests to declare.

Disclaimer. Publisher's note: Copernicus Publications remains neutral with regard to jurisdictional claims made in the text, published maps, institutional affiliations, or any other geographical representation in this paper. While Copernicus Publications makes every effort to include appropriate place names, the final responsibility lies with the authors.

Acknowledgements. The samples were collected using the FAAM BAe-146-301 Atmospheric Research Aircraft, flown by Airtask Ltd., maintained by Avalon Aero Ltd. and managed by the FAAM Airborne Laboratory. The FAAM Airborne Laboratory is jointly operated by UK Research and Innovation and the University of Leeds. We are grateful to all individuals from the Met Office, the University of Leeds, the University of Manchester, FAAM, Airtask and Avalon Aero who were instrumental in making the ACAO campaign a success. This work used JASMIN, the UK collaborative data analysis facility. We thank Alberto Sanchez-Marroquin (now at the Barcelona Supercomputing Center) for assistance with the scanning electron microscopy analysis. We acknowledge the use of imagery provided by services from NASA's Global Imagery Browse Services (GIBS), part of NASA's Earth Observing System Data and Information System (EOSDIS). We thank Armin Sorooshian and the anonymous reviewer for insightful comments that significantly improved this work. Additionally, we thank Cameron Belton for alerting us to typographical errors in the original manuscript.

We acknowledge the use of reanalysis data provided by the Copernicus Climate Change Service 2020.

Financial support. The ACAO flight campaign was largely funded by the Met Office, with a contribution of additional flight hours from M-Phase. M-Phase was supported by the Natural Environment Research Council (NERC) as part of the CloudSense programme (M-Phase (grant nos. NE/T00648X/1 NE/T006463/1), DCMEX (grant no. NE/T006420/1)). Erin N. Raif was supported by the NERC Panorama Doctoral Training Partnership with additional CASE sponsorship from the Met Office (grant no. NE/S007458/1). Sarah L. Barr was funded by an Industrial CASE studentship from NERC (grant no. NE/R006687/1).

Review statement. This paper was edited by Radovan Krejci and reviewed by Armin Sorooshian and one anonymous referee.

References

Abel, S. J., Cotton, R. J., Barrett, P. A., and Vance, A. K.: A comparison of ice water content measurement techniques on the FAAM BAe-146 aircraft, Atmos. Meas. Tech., 7, 3007–3022, https://doi.org/10.5194/amt-7-3007-2014, 2014.

Abel, S. J., Boutle, I. A., Waite, K., Fox, S., Brown, P. R. A., Cotton, R., Lloyd, G., Choularton, T. W., and Bower, K. N.: The Role of Precipitation in Controlling the Transition from Stratocumulus to Cumulus Clouds in a Northern Hemisphere Cold-Air Outbreak, J. Atmos. Sci., 74, 2293–2314, https://doi.org/10.1175/JAS-D-16-0362.1, 2017.

Andreae, M. O., Berresheim, H., Andreae, T. W., Kritz, M. A., Bates, T. S., and Merrill, J. T.: Vertical distribution of dimethylsulfide, sulfur dioxide, aerosol ions, and radon over the Northeast Pacific Ocean, J. Atmos. Chem., 6, 149–173, https://doi.org/10.1007/BF00048337, 1988.

Andreae, M. O., Elbert, W., Gabriel, R., Johnson, D. W., Osborne, S., and Wood, R.: Soluble ion chemistry of the atmospheric aerosol and SO_2 concentrations over the eastern North Atlantic during ACE-2, Tellus B, 52, 1066–1087, https://doi.org/10.3402/tellusb.v52i4.17087, 2000.

Ansmann, A., Ohneiser, K., Engelmann, R., Radenz, M., Griesche, H., Hofer, J., Althausen, D., Creamean, J. M., Boyer, M. C., Knopf, D. A., Dahlke, S., Maturilli, M., Gebauer, H., Bühl, J., Jimenez, C., Seifert, P., and Wandinger, U.: Annual cycle of aerosol properties over the central Arctic during MOSAiC 2019–2020 – light-extinction, CCN, and INP levels from the boundary layer to the tropopause, Atmos. Chem. Phys., 23, 12821–12849, https://doi.org/10.5194/acp-23-12821-2023, 2023.

Arteaga, D., Planche, C., Tridon, F., Dupuy, R., Baudoux, A., Banson, S., Baray, J.-L., Mioche, G., Ehrlich, A., Mech, M., Mertes, S., Wendisch, M., Wobrock, W., and Jourdan, O.: Arctic mixed-phase clouds simulated by the WRF model: Comparisons with ACLOUD radar and *in situ* airborne observations and sensitivity of microphysics properties, Atmos. Res., 307, 107 471, https://doi.org/10.1016/j.atmosres.2024.107471, 2024.

Barr, S. L.: The sources and activity of ice-nucleating particles in the high latitudes, PhD thesis, University of Leeds, https://etheses.whiterose.ac.uk/33752/ (last access: 30 November 2024), 2023.

Barr, S. L., Wyld, B., McQuaid, J. B., Neely III, R. R., and Murray, B. J.: Southern Alaska as a source of atmospheric mineral dust

and ice-nucleating particles, Science Advances, 9, eadg3708, https://doi.org/10.1126/sciadv.adg3708, 2023.

Barrett, P. A., Blyth, A., Brown, P. R. A., and Abel, S. J.: The structure of turbulence and mixed-phase cloud microphysics in a highly supercooled altocumulus cloud, Atmos. Chem. Phys., 20, 1921–1939, https://doi.org/10.5194/acp-20-1921-2020, 2020.

Barrie, L. A.: Arctic air pollution: An overview of current knowledge, Atmos. Environ., 20, 643–663, https://doi.org/10.1016/0004-6981(86)90180-0, 1986.

Beall, C. M., Lucero, D., Hill, T. C., DeMott, P. J., Stokes, M. D., and Prather, K. A.: Best practices for precipitation sample storage for offline studies of ice nucleation in marine and coastal environments, Atmos. Meas. Tech., 13, 6473–6486, https://doi.org/10.5194/amt-13-6473-2020, 2020.

Bergeron, T.: On the Physics of Cloud and Precipitation, Nippon Sugaku-Buturigakkwaishi, The Physical Society of Japan, 9, 446–448, https://doi.org/10.11429/subutsukaishi1927.9.446, 1935.

Bigg, E. K. and Leck, C.: Cloud-active particles over the central Arctic Ocean, J. Geophys. Res.-Atmos., 106, 32155–32166, https://doi.org/10.1029/1999JD901152, 2001.

Borys, R. D.: Studies of ice nucleation by Arctic aerosol on AGASP-II, J. Atmos. Chem., 9, 169–185, https://doi.org/10.1007/BF00052831, 1989.

Brasseur, Z., Castarède, D., Thomson, E. S., Adams, M. P., Drossaart van Dusseldorp, S., Heikkilä, P., Korhonen, K., Lampilahti, J., Paramonov, M., Schneider, J., Vogel, F., Wu, Y., Abbatt, J. P. D., Atanasova, N. S., Bamford, D. H., Bertozzi, B., Boyer, M., Brus, D., Daily, M. I., Fösig, R., Gute, E., Harrison, A. D., Hietala, P., Höhler, K., Kanji, Z. A., Keskinen, J., Lacher, L., Lampimäki, M., Levula, J., Manninen, A., Nadolny, J., Peltola, M., Porter, G. C. E., Poutanen, P., Proske, U., Schorr, T., Silas Umo, N., Stenszky, J., Virtanen, A., Moisseev, D., Kulmala, M., Murray, B. J., Petäjä, T., Möhler, O., and Duplissy, J.: Measurement report: Introduction to the HyICE-2018 campaign for measurements of ice-nucleating particles and instrument inter-comparison in the Hyytiälä boreal forest, Atmos. Chem. Phys., 22, 5117–5145, https://doi.org/10.5194/acp-22-5117-2022, 2022.

Brümmer, B.: Boundary-layer modification in wintertime cold-air outbreaks from the Arctic sea ice, Bound.-Lay. Meteorol., 80, 109–125, https://doi.org/10.1007/BF00119014, 1996.

Bullard, J. E., Baddock, M., Bradwell, T., Crusius, J., Darlington, E., Gaiero, D., Gassó, S., Gisladottir, G., Hodgkins, R., McCulloch, R., McKenna-Neuman, C., Mockford, T., Stewart, H., and Thorsteinsson, T.: High-latitude dust in the Earth system, Rev. Geophys., 54, 447–485, https://doi.org/10.1002/2016RG000518, 2016.

C3S: ERA5 hourly data on single levels from 1940 to present, Copernicus Climate Data Store [data set], https://doi.org/10.24381/CDS.ADBB2D47, 2018.

Carlsen, T. and David, R. O.: Spaceborne Evidence That Ice-Nucleating Particles Influence High-Latitude Cloud Phase, Geophys. Res. Lett., 49, e2022GL098041, https://doi.org/10.1029/2022GL098041, 2022.

Carslaw, K. S.: Chapter 5 – Aerosol processes, in: Aerosols and Climate, edited by: Carslaw, K. S., 135–185, Elsevier, ISBN 978-0-12-819766-0, https://doi.org/10.1016/B978-0-12-819766-0.00007-9, 2022.

Chen, J., Wu, Z., Chen, J., Reicher, N., Fang, X., Rudich, Y., and Hu, M.: Size-resolved atmospheric ice-nucleating particles during East Asian dust events, Atmos. Chem. Phys., 21, 3491–3506, https://doi.org/10.5194/acp-21-3491-2021, 2021.

Creamean, J. M., Suski, K. J., Rosenfeld, D., Cazorla, A., DeMott, P. J., Sullivan, R. C., White, A. B., Ralph, F. M., Minnis, P., Comstock, J. M., Tomlinson, J. M., and Prather, K. A.: Dust and Biological Aerosols from the Sahara and Asia Influence Precipitation in the Western U.S., Science, 339, 1572–1578, https://doi.org/10.1126/science.1227279, 2013.

Creamean, J. M., Hill, T. C. J., DeMott, P. J., Uetake, J., Kreidenweis, S., and Douglas, T. A.: Thawing permafrost: an overlooked source of seeds for Arctic cloud formation, Environ. Res. Lett., 15, 084022, https://doi.org/10.1088/1748-9326/ab87d3, 2020.

Creamean, J. M., Barry, K., Hill, T. C. J., Hume, C., DeMott, P. J., Shupe, M. D., Dahlke, S., Willmes, S., Schmale, J., Beck, I., Hoppe, C. J. M., Fong, A., Chamberlain, E., Bowman, J., Scharien, R., and Persson, O.: Annual cycle observations of aerosols capable of ice formation in central Arctic clouds, Nat. Commun., 13, 3537, https://doi.org/10.1038/s41467-022-31182-x, 2022.

DeMott, P. J., Hill, T. C. J., McCluskey, C. S., Prather, K. A., Collins, D. B., Sullivan, R. C., Ruppel, M. J., Mason, R. H., Irish, V. E., Lee, T., Hwang, C. Y., Rhee, T. S., Snider, J. R., McMeeking, G. R., Dhaniyala, S., Lewis, E. R., Wentzell, J. J. B., Abbatt, J., Lee, C., Sultana, C. M., Ault, A. P., Axson, J. L., Diaz Martinez, M., Venero, I., Santos-Figueroa, G., Stokes, M. D., Deane, G. B., Mayol-Bracero, O. L., Grassian, V. H., Bertram, T. H., Bertram, A. K., Moffett, B. F., and Franc, G. D.: Sea spray aerosol as a unique source of ice nucleating particles, P. Natl. Acad. Sci. USA, 113, 5797–5803, https://doi.org/10.1073/pnas.1514034112, 2016.

DeMott, P. J., Möhler, O., Cziczo, D. J., Hiranuma, N., Petters, M. D., Petters, S. S., Belosi, F., Bingemer, H. G., Brooks, S. D., Budke, C., Burkert-Kohn, M., Collier, K. N., Danielczok, A., Eppers, O., Felgitsch, L., Garimella, S., Grothe, H., Herenz, P., Hill, T. C. J., Höhler, K., Kanji, Z. A., Kiselev, A., Koop, T., Kristensen, T. B., Krüger, K., Kulkarni, G., Levin, E. J. T., Murray, B. J., Nicosia, A., O'Sullivan, D., Peckhaus, A., Polen, M. J., Price, H. C., Reicher, N., Rothenberg, D. A., Rudich, Y., Santachiara, G., Schiebel, T., Schrod, J., Seifried, T. M., Stratmann, F., Sullivan, R. C., Suski, K. J., Szakáll, M., Taylor, H. P., Ullrich, R., Vergara-Temprado, J., Wagner, R., Whale, T. F., Weber, D., Welti, A., Wilson, T. W., Wolf, M. J., and Zenker, J.: The Fifth International Workshop on Ice Nucleation phase 2 (FIN-02): laboratory intercomparison of ice nucleation measurements, Atmos. Meas. Tech., 11, 6231–6257, https://doi.org/10.5194/amt-11-6231-2018, 2018.

Dörnbrack, A., Stachlewska, I. S., Ritter, C., and Neuber, R.: Aerosol distribution around Svalbard during intense easterly winds, Atmos. Chem. Phys., 10, 1473–1490, https://doi.org/10.5194/acp-10-1473-2010, 2010.

Ekman, A. M. L. and Schmale, J.: Chapter 16 – Aerosol processes in high-latitude environments and the effects on climate, in: Aerosols and Climate, edited by: Carslaw, K. S., Elsevier, 651–706, ISBN 978-0-12-819766-0, https://doi.org/10.1016/B978-0-12-819766-0.00005-5, 2022.

Facility for Airborne and Atmospheric Measurements: Arctic Cold Air Outbreak (ACAO) FAAM Project, Centre for Environmen-

tal Data Analysis [data set], https://catalogue.ceda.ac.uk/uuid/01021a90c0c2481c909bdb145cb72398 (last access: 2 December 2024), 2024.

Field, P. R., Lawson, R. P., Brown, P. R. A., Lloyd, G., Westbrook, C., Moisseev, D., Miltenberger, A., Nenes, A., Blyth, A., Choularton, T., Connolly, P., Buehl, J., Crosier, J., Cui, Z., Dearden, C., DeMott, P., Flossmann, A., Heymsfield, A., Huang, Y., Kalesse, H., Kanji, Z. A., Korolev, A., Kirchgaessner, A., Lasher-Trapp, S., Leisner, T., McFarquhar, G., Phillips, V., Stith, J., and Sullivan, S.: Secondary Ice Production: Current State of the Science and Recommendations for the Future, Meteor. Mon., 58, 7.1–7.20, https://doi.org/10.1175/AMSMONOGRAPHS-D-16-0014.1, 2017.

Findeisen, W.: Die kolloidmeteorolgischen Vorgänge bei der Niederschlagsbildung, Meteorol. Z., 55, 121–133, 1938.

Fletcher, J., Mason, S., and Jakob, C.: The Climatology, Meteorology, and Boundary Layer Structure of Marine Cold Air Outbreaks in Both Hemispheres, J. Climate, 29, 1999–2014, https://doi.org/10.1175/JCLI-D-15-0268.1, 2016a.

Fletcher, J. K., Mason, S., and Jakob, C.: A Climatology of Clouds in Marine Cold Air Outbreaks in Both Hemispheres, J. Climate, 29, 6677–6692, https://doi.org/10.1175/JCLI-D-15-0783.1, 2016b.

Garrett, T. J., Hobbs, P. V., and Gerber, H.: Shortwave, single-scattering properties of arctic ice clouds, J. Geophys. Res.-Atmos., 106, 15155–15172, https://doi.org/10.1029/2000JD900195, 2001.

Geerts, B., Giangrande, S. E., McFarquhar, G. M., Xue, L., Abel, S. J., Comstock, J. M., Crewell, S., DeMott, P. J., Ebell, K., Field, P., Hill, T. C. J., Hunzinger, A., Jensen, M. P., Johnson, K. L., Juliano, T. W., Kollias, P., Kosovic, B., Lackner, C., Luke, E., Lüpkes, C., Matthews, A. A., Neggers, R., Ovchinnikov, M., Powers, H., Shupe, M. D., Spengler, T., Swanson, B. E., Tjernström, M., Theisen, A. K., Wales, N. A., Wang, Y., Wendisch, M., and Wu, P.: The COMBLE Campaign: A Study of Marine Boundary Layer Clouds in Arctic Cold-Air Outbreaks, B. Am. Meteorol. Soc., 103, E1371–E1389, https://doi.org/10.1175/BAMS-D-21-0044.1, 2022.

Gjelsvik, A. B., David, R. O., Carlsen, T., Hellmuth, F., Hofer, S., McGraw, Z., Sodemann, H., and Storelvmo, T.: Using a region-specific ice-nucleating particle parameterization improves the representation of Arctic clouds in a global climate model, EGUsphere [preprint], https://doi.org/10.5194/egusphere-2024-1879, 2024.

Gong, X., Zhang, J., Croft, B., Yang, X., Frey, M. M., Bergner, N., Chang, R. Y.-W., Creamean, J. M., Kuang, C., Martin, R. V., Ranjithkumar, A., Sedlacek, A. J., Uin, J., Willmes, S., Zawadowicz, M. A., Pierce, J. R., Shupe, M. D., Schmale, J., and Wang, J.: Arctic warming by abundant fine sea salt aerosols from blowing snow, Nat. Geosci., 16, 768–774, https://doi.org/10.1038/s41561-023-01254-8, 2023.

Groot Zwaaftink, C. D., Grythe, H., Skov, H., and Stohl, A.: Substantial contribution of northern high-latitude sources to mineral dust in the Arctic, J. Geophys. Res.-Atmos., 121, 13678–13697, https://doi.org/10.1002/2016JD025482, 2016.

Hallett, J. and Mossop, S. C.: Production of secondary ice particles during the riming process, Nature, 249, 26–28, https://doi.org/10.1038/249026a0, 1974.

Harrison, A. D., Lever, K., Sanchez-Marroquin, A., Holden, M. A., Whale, T. F., Tarn, M. D., McQuaid, J. B., and Murray, B. J.: The ice-nucleating ability of quartz immersed in water and its atmospheric importance compared to K-feldspar, Atmos. Chem. Phys., 19, 11343–11361, https://doi.org/10.5194/acp-19-11343-2019, 2019.

Hartmann, M., Adachi, K., Eppers, O., Haas, C., Herber, A., Holzinger, R., Hünerbein, A., Jäkel, E., Jentzsch, C., van Pinxteren, M., Wex, H., Willmes, S., and Stratmann, F.: Wintertime Airborne Measurements of Ice Nucleating Particles in the High Arctic: A Hint to a Marine, Biogenic Source for Ice Nucleating Particles, Geophys. Res. Lett., 47, e2020GL087770, https://doi.org/10.1029/2020GL087770, 2020.

Hartmann, M., Gong, X., Kecorius, S., van Pinxteren, M., Vogl, T., Welti, A., Wex, H., Zeppenfeld, S., Herrmann, H., Wiedensohler, A., and Stratmann, F.: Terrestrial or marine – indications towards the origin of ice-nucleating particles during melt season in the European Arctic up to 83.7° N, Atmos. Chem. Phys., 21, 11613–11636, https://doi.org/10.5194/acp-21-11613-2021, 2021.

Herbert, R. J., Murray, B. J., Dobbie, S. J., and Koop, T.: Sensitivity of liquid clouds to homogenous freezing parameterizations, Geophys. Res. Lett., 42, 1599–1605, https://doi.org/10.1002/2014GL062729, 2015.

Hiranuma, N., Adachi, K., Bell, D. M., Belosi, F., Beydoun, H., Bhaduri, B., Bingemer, H., Budke, C., Clemen, H.-C., Conen, F., Cory, K. M., Curtius, J., DeMott, P. J., Eppers, O., Grawe, S., Hartmann, S., Hoffmann, N., Höhler, K., Jantsch, E., Kiselev, A., Koop, T., Kulkarni, G., Mayer, A., Murakami, M., Murray, B. J., Nicosia, A., Petters, M. D., Piazza, M., Polen, M., Reicher, N., Rudich, Y., Saito, A., Santachiara, G., Schiebel, T., Schill, G. P., Schneider, J., Segev, L., Stopelli, E., Sullivan, R. C., Suski, K., Szakáll, M., Tajiri, T., Taylor, H., Tobo, Y., Ullrich, R., Weber, D., Wex, H., Whale, T. F., Whiteside, C. L., Yamashita, K., Zelenyuk, A., and Möhler, O.: A comprehensive characterization of ice nucleation by three different types of cellulose particles immersed in water, Atmos. Chem. Phys., 19, 4823–4849, https://doi.org/10.5194/acp-19-4823-2019, 2019.

Huang, S., Hu, W., Chen, J., Wu, Z., Zhang, D., and Fu, P.: Overview of biological ice nucleating particles in the atmosphere, Environ. Int., 146, 106197, https://doi.org/10.1016/j.envint.2020.106197, 2021.

Ickes, L., Welti, A., Hoose, C., and Lohmann, U.: Classical nucleation theory of homogeneous freezing of water: thermodynamic and kinetic parameters, Phys. Chem. Chem. Phys., 17, 5514–5537, https://doi.org/10.1039/C4CP04184D, 2015.

Kanji, Z. A., Ladino, L. A., Wex, H., Boose, Y., Burkert-Kohn, M., Cziczo, D. J., and Krämer, M.: Overview of Ice Nucleating Particles, Meteor. Mon., 58, 1.1–1.33, https://doi.org/10.1175/AMSMONOGRAPHS-D-16-0006.1, 2017.

Kawai, K., Matsui, H., and Tobo, Y.: Dominant Role of Arctic Dust With High Ice Nucleating Ability in the Arctic Lower Troposphere, Geophys. Res. Lett., 50, e2022GL102470, https://doi.org/10.1029/2022GL102470, 2023.

Knopf, D. A., Wang, P., Wong, B., Tomlin, J. M., Veghte, D. P., Lata, N. N., China, S., Laskin, A., Moffet, R. C., Aller, J. Y., Marcus, M. A., and Wang, J.: Physicochemical characterization of free troposphere and marine boundary layer ice-nucleating particles collected by aircraft in the eastern North Atlantic, At-

mos. Chem. Phys., 23, 8659–8681, https://doi.org/10.5194/acp-23-8659-2023, 2023.

Korolev, A. and Leisner, T.: Review of experimental studies of secondary ice production, Atmos. Chem. Phys., 20, 11767–11797, https://doi.org/10.5194/acp-20-11767-2020, 2020.

Korolev, A., McFarquhar, G., Field, P. R., Franklin, C., Lawson, P., Wang, Z., Williams, E., Abel, S. J., Axisa, D., Borrmann, S., Crosier, J., Fugal, J., Krämer, M., Lohmann, U., Schlenczek, O., Schnaiter, M., and Wendisch, M.: Mixed-Phase Clouds: Progress and Challenges, Meteor. Mon., 58, 5.1–5.50, https://doi.org/10.1175/AMSMONOGRAPHS-D-17-0001.1, 2017.

Korolev, A. V., Strapp, J. W., Isaac, G. A., and Nevzorov, A. N.: The Nevzorov Airborne Hot-Wire LWC–TWC Probe: Principle of Operation and Performance Characteristics, J. Atmos. Ocean. Tech., 15, 1495–1510, https://doi.org/10.1175/1520-0426(1998)015<1495:TNAHWL>2.0.CO;2, 1998.

Lacher, L., Adams, M. P., Barry, K., Bertozzi, B., Bingemer, H., Boffo, C., Bras, Y., Büttner, N., Castarede, D., Cziczo, D. J., DeMott, P. J., Fösig, R., Goodell, M., Höhler, K., Hill, T. C. J., Jentzsch, C., Ladino, L. A., Levin, E. J. T., Mertes, S., Möhler, O., Moore, K. A., Murray, B. J., Nadolny, J., Pfeuffer, T., Picard, D., Ramírez-Romero, C., Ribeiro, M., Richter, S., Schrod, J., Sellegri, K., Stratmann, F., Swanson, B. E., Thomson, E. S., Wex, H., Wolf, M. J., and Freney, E.: The Puy de Dôme ICe Nucleation Intercomparison Campaign (PICNIC): comparison between online and offline methods in ambient air, Atmos. Chem. Phys., 24, 2651–2678, https://doi.org/10.5194/acp-24-2651-2024, 2024.

Latimer, R. N. C. and Martin, R. V.: Interpretation of measured aerosol mass scattering efficiency over North America using a chemical transport model, Atmos. Chem. Phys., 19, 2635–2653, https://doi.org/10.5194/acp-19-2635-2019, 2019.

Li, G., Wilbourn, E. K., Cheng, Z., Wieder, J., Fagerson, A., Henneberger, J., Motos, G., Traversi, R., Brooks, S. D., Mazzola, M., China, S., Nenes, A., Lohmann, U., Hiranuma, N., and Kanji, Z. A.: Physicochemical characterization and source apportionment of Arctic ice-nucleating particles observed in Ny-Ålesund in autumn 2019, Atmos. Chem. Phys., 23, 10489–10516, https://doi.org/10.5194/acp-23-10489-2023, 2023.

Liu, D., Quennehen, B., Darbyshire, E., Allan, J. D., Williams, P. I., Taylor, J. W., Bauguitte, S. J.-B., Flynn, M. J., Lowe, D., Gallagher, M. W., Bower, K. N., Choularton, T. W., and Coe, H.: The importance of Asia as a source of black carbon to the European Arctic during springtime 2013, Atmos. Chem. Phys., 15, 11537–11555, https://doi.org/10.5194/acp-15-11537-2015, 2015.

Martin, R. V., Jacob, D. J., Yantosca, R. M., Chin, M., and Ginoux, P.: Global and regional decreases in tropospheric oxidants from photochemical effects of aerosols, J. Geophys. Res.-Atmos., 108, 4097, https://doi.org/10.1029/2002JD002622, 2003.

McCluskey, C. S., Hill, T. C. J., Humphries, R. S., Rauker, A. M., Moreau, S., Strutton, P. G., Chambers, S. D., Williams, A. G., McRobert, I., Ward, J., Keywood, M. D., Harnwell, J., Ponsonby, W., Loh, Z. M., Krummel, P. B., Protat, A., Kreidenweis, S. M., and DeMott, P. J.: Observations of Ice Nucleating Particles Over Southern Ocean Waters, Geophys. Res. Lett., 45, 11989–11997, https://doi.org/10.1029/2018GL079981, 2018a.

McCluskey, C. S., Ovadnevaite, J., Rinaldi, M., Atkinson, J., Belosi, F., Ceburnis, D., Marullo, S., Hill, T. C. J., Lohmann, U., Kanji, Z. A., O'Dowd, C., Kreidenweis, S. M., and DeMott, P. J.: Marine and Terrestrial Organic Ice-Nucleating Particles in Pristine Marine to Continentally Influenced Northeast Atlantic Air Masses, J. Geophys. Res.-Atmos., 123, 6196–6212, https://doi.org/10.1029/2017JD028033, 2018b.

McFarquhar, G. M., Bretherton, C. S., Marchand, R., Protat, A., DeMott, P. J., Alexander, S. P., Roberts, G. C., Twohy, C. H., Toohey, D., Siems, S., Huang, Y., Wood, R., Rauber, R. M., Lasher-Trapp, S., Jensen, J., Stith, J. L., Mace, J., Um, J., Järvinen, E., Schnaiter, M., Gettelman, A., Sanchez, K. J., McCluskey, C. S., Russell, L. M., McCoy, I. L., Atlas, R. L., Bardeen, C. G., Moore, K. A., Hill, T. C. J., Humphries, R. S., Keywood, M. D., Ristovski, Z., Cravigan, L., Schofield, R., Fairall, C., Mallet, M. D., Kreidenweis, S. M., Rainwater, B., D'Alessandro, J., Wang, Y., Wu, W., Saliba, G., Levin, E. J. T., Ding, S., Lang, F., Truong, S. C. H., Wolff, C., Haggerty, J., Harvey, M. J., Klekociuk, A. R., and McDonald, A.: Observations of Clouds, Aerosols, Precipitation, and Surface Radiation over the Southern Ocean: An Overview of Capricorn, Marcus, Micre, and Socrates, B. Am. Meteorol. Soc., 102, E894–E928, https://doi.org/10.1175/BAMS-D-20-0132.1, 2021.

Meinander, O., Dagsson-Waldhauserova, P., Amosov, P., Aseyeva, E., Atkins, C., Baklanov, A., Baldo, C., Barr, S. L., Barzycka, B., Benning, L. G., Cvetkovic, B., Enchilik, P., Frolov, D., Gassó, S., Kandler, K., Kasimov, N., Kavan, J., King, J., Koroleva, T., Krupskaya, V., Kulmala, M., Kusiak, M., Lappalainen, H. K., Laska, M., Lasne, J., Lewandowski, M., Luks, B., McQuaid, J. B., Moroni, B., Murray, B., Möhler, O., Nawrot, A., Nickovic, S., O'Neill, N. T., Pejanovic, G., Popovicheva, O., Ranjbar, K., Romanias, M., Samonova, O., Sanchez-Marroquin, A., Schepanski, K., Semenkov, I., Sharapova, A., Shevnina, E., Shi, Z., Sofiev, M., Thevenet, F., Thorsteinsson, T., Timofeev, M., Umo, N. S., Uppstu, A., Urupina, D., Varga, G., Werner, T., Arnalds, O., and Vukovic Vimic, A.: Newly identified climatically and environmentally significant high-latitude dust sources, Atmos. Chem. Phys., 22, 11889–11930, https://doi.org/10.5194/acp-22-11889-2022, 2022.

MODIS Land Science Team: MODIS/Terra Atmospherically Corrected Surface Reflectance 5-Min L2 Swath 250m, 500m, 1km, Level-1 and Atmosphere Archive & Distribution System Distributed Active Archive Center [data set], https://doi.org/10.5067/MODIS/MOD09.061, 2020.

Moore, K. A., Hill, T. C. J., McCluskey, C. S., Twohy, C. H., Rainwater, B., Toohey, D. W., Sanchez, K. J., Kreidenweis, S. M., and DeMott, P. J.: Characterizing Ice Nucleating Particles Over the Southern Ocean Using Simultaneous Aircraft and Ship Observations, J. Geophys. Res.-Atmos., 129, e2023JD039 543, https://doi.org/10.1029/2023JD039543, 2024.

Morrison, H., de Boer, G., Feingold, G., Harrington, J., Shupe, M. D., and Sulia, K.: Resilience of persistent Arctic mixed-phase clouds, Nat. Geosci., 5, 11–17, https://doi.org/10.1038/ngeo1332, 2012.

Murray, B. J., Haddrell, A. E., Peppe, S., Davies, J. F., Reid, J. P., O'Sullivan, D., Price, H. C., Kumar, R., Saunders, R. W., Plane, J. M. C., Umo, N. S., and Wilson, T. W.: Glass formation and unusual hygroscopic growth of iodic acid solution droplets with relevance for iodine mediated particle formation in the marine boundary layer, Atmos. Chem. Phys., 12, 8575–8587, https://doi.org/10.5194/acp-12-8575-2012, 2012a.

Murray, B. J., O'Sullivan, D., Atkinson, J. D., and Webb, M. E.: Ice nucleation by particles immersed in supercooled cloud droplets, Chem. Soc. Rev., 41, 6519–6554, https://doi.org/10.1039/C2CS35200A, 2012b.

Murray, B. J., Carslaw, K. S., and Field, P. R.: Opinion: Cloud-phase climate feedback and the importance of ice-nucleating particles, Atmos. Chem. Phys., 21, 665–679, https://doi.org/10.5194/acp-21-665-2021, 2021.

Murray-Watson, R. J. and Gryspeerdt, E.: Air mass history linked to the development of Arctic mixed-phase clouds, Atmos. Chem. Phys., 24, 11115–11132, https://doi.org/10.5194/acp-24-11115-2024, 2024.

Murray-Watson, R. J., Gryspeerdt, E., and Goren, T.: Investigating the development of clouds within marine cold-air outbreaks, Atmos. Chem. Phys., 23, 9365–9383, https://doi.org/10.5194/acp-23-9365-2023, 2023.

Niemand, M., Möhler, O., Vogel, B., Vogel, H., Hoose, C., Connolly, P., Klein, H., Bingemer, H., DeMott, P., Skrotzki, J., and Leisner, T.: A Particle-Surface-Area-Based Parameterization of Immersion Freezing on Desert Dust Particles, J. Atmos. Sci., 69, 3077–3092, https://doi.org/10.1175/JAS-D-11-0249.1, 2012.

O'Sullivan, D., Adams, M. P., Tarn, M. D., Harrison, A. D., Vergara-Temprado, J., Porter, G. C. E., Holden, M. A., Sanchez-Marroquin, A., Carotenuto, F., Whale, T. F., McQuaid, J. B., Walshaw, R., Hedges, D. H. P., Burke, I. T., Cui, Z., and Murray, B. J.: Contributions of biogenic material to the atmospheric ice-nucleating particle population in North Western Europe, Sci. Rep., 8, 13821, https://doi.org/10.1038/s41598-018-31981-7, 2018.

Pereira Freitas, G., Adachi, K., Conen, F., Heslin-Rees, D., Krejci, R., Tobo, Y., Yttri, K. E., and Zieger, P.: Regionally sourced bioaerosols drive high-temperature ice nucleating particles in the Arctic, Nat. Commun., 14, 5997, https://doi.org/10.1038/s41467-023-41696-7, 2023.

Petters, M. D. and Wright, T. P.: Revisiting ice nucleation from precipitation samples, Geophys. Res. Lett., 42, 8758–8766, https://doi.org/10.1002/2015GL065733, 2015.

Pithan, F., Svensson, G., Caballero, R., Chechin, D., Cronin, T. W., Ekman, A. M. L., Neggers, R., Shupe, M. D., Solomon, A., Tjernström, M., and Wendisch, M.: Role of air-mass transformations in exchange between the Arctic and mid-latitudes, Nat. Geosci., 11, 805–812, https://doi.org/10.1038/s41561-018-0234-1, 2018.

Porter, G. C. E., Adams, M. P., Brooks, I. M., Ickes, L., Karlsson, L., Leck, C., Salter, M. E., Schmale, J., Siegel, K., Sikora, S. N. F., Tarn, M. D., Vüllers, J., Wernli, H., Zieger, P., Zinke, J., and Murray, B. J.: Highly Active Ice-Nucleating Particles at the Summer North Pole, J. Geophys. Res.-Atmos., 127, e2021JD036059, https://doi.org/10.1029/2021JD036059, 2022.

Prenni, A. J., Harrington, J. Y., Tjernström, M., DeMott, P. J., Avramov, A., Long, C. N., Kreidenweis, S. M., Olsson, P. Q., and Verlinde, J.: Can Ice-Nucleating Aerosols Affect Arctic Seasonal Climate?, B. Am. Meteorol. Soc., 88, 541–550, https://doi.org/10.1175/BAMS-88-4-541, 2007.

Price, H. C., Baustian, K. J., McQuaid, J. B., Blyth, A., Bower, K. N., Choularton, T., Cotton, R. J., Cui, Z., Field, P. R., Gallagher, M., Hawker, R., Merrington, A., Miltenberger, A., Neely III, R. R., Parker, S. T., Rosenberg, P. D., Taylor, J. W., Trembath, J., Vergara-Temprado, J., Whale, T. F., Wilson, T. W., Young, G., and Murray, B. J.: Atmospheric Ice-Nucleating Particles in the Dusty Tropical Atlantic, J. Geophys. Res.-Atmos., 123, 2175–2193, https://doi.org/10.1002/2017JD027560, 2018.

Rahn, K. A., Borys, R. D., and Shaw, G. E.: The Asian source of Arctic haze bands, Nature, 268, 713–715, https://doi.org/10.1038/268713a0, 1977.

Raif, E.: erin-raif/acao_inp_arctic_haze: Preprint after reviewer response (v0.2), Zenodo, https://doi.org/10.5281/zenodo.11221398, 2024.

Raif, E., Daily, M., Abel, S., Barr, S., Tarn, M., McQuaid, J., Barrett, P., Bower, K., Field, P., Carslaw, K., and Murray, B.: Data and metadata associated with ice-nucleating particles during the 2022 Arctic Cold Air Outbreak Campaign, Zenodo [data set], https://doi.org/10.5281/zenodo.11221599, 2024.

Rinaldi, M., Hiranuma, N., Santachiara, G., Mazzola, M., Mansour, K., Paglione, M., Rodriguez, C. A., Traversi, R., Becagli, S., Cappelletti, D., and Belosi, F.: Ice-nucleating particle concentration measurements from Ny-Ålesund during the Arctic spring–summer in 2018, Atmos. Chem. Phys., 21, 14725–14748, https://doi.org/10.5194/acp-21-14725-2021, 2021.

Rogers, D. C., DeMott, P. J., and Kreidenweis, S. M.: Airborne measurements of tropospheric ice-nucleating aerosol particles in the Arctic spring, J. Geophys. Res.-Atmos., 106, 15053–15063, https://doi.org/10.1029/2000JD900790, 2001.

Rosenberg, P. D., Dean, A. R., Williams, P. I., Dorsey, J. R., Minikin, A., Pickering, M. A., and Petzold, A.: Particle sizing calibration with refractive index correction for light scattering optical particle counters and impacts upon PCASP and CDP data collected during the Fennec campaign, Atmos. Meas. Tech., 5, 1147–1163, https://doi.org/10.5194/amt-5-1147-2012, 2012.

Rymer, K. G., Rachlewicz, G., Buchwal, A., Temme, A. J. A. M., Reimann, T., and van der Meij, W. M.: Contemporary and past aeolian deposition rates in periglacial conditions (Ebba Valley, central Spitsbergen), CATENA, 211, 105974, https://doi.org/10.1016/j.catena.2021.105974, 2022.

Sanchez-Marroquin, A., Hedges, D. H. P., Hiscock, M., Parker, S. T., Rosenberg, P. D., Trembath, J., Walshaw, R., Burke, I. T., McQuaid, J. B., and Murray, B. J.: Characterisation of the filter inlet system on the FAAM BAe-146 research aircraft and its use for size-resolved aerosol composition measurements, Atmos. Meas. Tech., 12, 5741–5763, https://doi.org/10.5194/amt-12-5741-2019, 2019.

Sanchez-Marroquin, A., Arnalds, O., Baustian-Dorsi, K. J., Browse, J., Dagsson-Waldhauserova, P., Harrison, A. D., Maters, E. C., Pringle, K. J., Vergara-Temprado, J., Burke, I. T., McQuaid, J. B., Carslaw, K. S., and Murray, B. J.: Iceland is an episodic source of atmospheric ice-nucleating particles relevant for mixed-phase clouds, Science Advances, 6, eaba8137, https://doi.org/10.1126/sciadv.aba8137, 2020.

Sanchez-Marroquin, A., West, J. S., Burke, I. T., McQuaid, J. B., and Murray, B. J.: Mineral and biological ice-nucleating particles above the South East of the British Isles, Environmental Science: Atmospheres, 1, 176–191, https://doi.org/10.1039/D1EA00003A, 2021.

Sanchez-Marroquin, A., Barr, S. L., Burke, I. T., McQuaid, J. B., and Murray, B. J.: Aircraft ice-nucleating particle and aerosol composition measurements in the western North American Arctic, Atmos. Chem. Phys., 23, 13819–13834, https://doi.org/10.5194/acp-23-13819-2023, 2023.

Schmale, J., Baccarini, A., Thurnherr, I., Henning, S., Efraim, A., Regayre, L., Bolas, C., Hartmann, M., Welti, A., Lehtipalo, K., Aemisegger, F., Tatzelt, C., Landwehr, S., Modini, R. L., Tummon, F., Johnson, J. S., Harris, N., Schnaiter, M., Toffoli, A., Derkani, M., Bukowiecki, N., Stratmann, F., Dommen, J., Baltensperger, U., Wernli, H., Rosenfeld, D., Gysel-Beer, M., and Carslaw, K. S.: Overview of the Antarctic Circumnavigation Expedition: Study of Preindustrial-like Aerosols and Their Climate Effects (ACE-SPACE), B. Am. Meteorol. Soc., 100, 2260–2283, https://doi.org/10.1175/BAMS-D-18-0187.1, 2019.

Shaw, G. E.: The Arctic Haze Phenomenon, B. Am. Meteorol. Soc., 76, 2403–2414, https://doi.org/10.1175/1520-0477(1995)076<2403:TAHP>2.0.CO;2, 1995.

Shi, Y., Liu, X., Wu, M., Zhao, X., Ke, Z., and Brown, H.: Relative importance of high-latitude local and long-range-transported dust for Arctic ice-nucleating particles and impacts on Arctic mixed-phase clouds, Atmos. Chem. Phys., 22, 2909–2935, https://doi.org/10.5194/acp-22-2909-2022, 2022.

Song, C., Dall'Osto, M., Lupi, A., Mazzola, M., Traversi, R., Becagli, S., Gilardoni, S., Vratolis, S., Yttri, K. E., Beddows, D. C. S., Schmale, J., Brean, J., Kramawijaya, A. G., Harrison, R. M., and Shi, Z.: Differentiation of coarse-mode anthropogenic, marine and dust particles in the High Arctic islands of Svalbard, Atmos. Chem. Phys., 21, 11317–11335, https://doi.org/10.5194/acp-21-11317-2021, 2021.

Sorooshian, A., Anderson, B., Bauer, S. E., Braun, R. A., Cairns, B., Crosbie, E., Dadashazar, H., Diskin, G., Ferrare, R., Flagan, R. C., Hair, J., Hostetler, C., Jonsson, H. H., Kleb, M. M., Liu, H., MacDonald, A. B., McComiskey, A., Moore, R., Painemal, D., Russell, L. M., Seinfeld, J. H., Shook, M., Smith, W. L., Thornhill, K., Tselioudis, G., Wang, H., Zeng, X., Zhang, B., Ziemba, L., and Zuidema, P.: Aerosol–Cloud–Meteorology Interaction Airborne Field Investigations: Using Lessons Learned from the U.S. West Coast in the Design of ACTIVATE off the U.S. East Coast, B. Am. Meteorol. Soc., 100, 1511–1528, https://doi.org/10.1175/BAMS-D-18-0100.1, 2019.

Stein, A. F., Draxler, R. R., Rolph, G. D., Stunder, B. J. B., Cohen, M. D., and Ngan, F.: NOAA's HYSPLIT Atmospheric Transport and Dispersion Modeling System, B. Am. Meteorol. Soc., 96, 2059–2077, https://doi.org/10.1175/BAMS-D-14-00110.1, 2015.

Steinke, I., Funk, R., Busse, J., Iturri, A., Kirchen, S., Leue, M., Möhler, O., Schwartz, T., Schnaiter, M., Sierau, B., Toprak, E., Ullrich, R., Ulrich, A., Hoose, C., and Leisner, T.: Ice nucleation activity of agricultural soil dust aerosols from Mongolia, Argentina, and Germany, J. Geophys. Res.-Atmos., 121, 13559–13576, https://doi.org/10.1002/2016JD025160, 2016.

Stohl, A.: Characteristics of atmospheric transport into the Arctic troposphere, J. Geophys. Res.-Atmos., 111, D11306, https://doi.org/10.1029/2005JD006888, 2006.

Storelvmo, T., Tan, I., and Korolev, A. V.: Cloud Phase Changes Induced by CO_2 Warming – a Powerful yet Poorly Constrained Cloud-Climate Feedback, Current Climate Change Reports, 1, 288–296, https://doi.org/10.1007/s40641-015-0026-2, 2015.

Sze, K. C. H., Wex, H., Hartmann, M., Skov, H., Massling, A., Villanueva, D., and Stratmann, F.: Ice-nucleating particles in northern Greenland: annual cycles, biological contribution and parameterizations, Atmos. Chem. Phys., 23, 4741–4761, https://doi.org/10.5194/acp-23-4741-2023, 2023.

Talbot, R. W., Andreae, M. O., Berresheim, H., Artaxo, P., Garstang, M., Harriss, R. C., Beecher, K. M., and Li, S. M.: Aerosol chemistry during the wet season in central Amazonia: The influence of long-range transport, J. Geophys. Res.-Atmos., 95, 16955–16969, https://doi.org/10.1029/JD095iD10p16955, 1990.

Tang, I. N., Tridico, A. C., and Fung, K. H.: Thermodynamic and optical properties of sea salt aerosols, J. Geophys. Res.-Atmos., 102, 23269–23275, https://doi.org/10.1029/97JD01806, 1997.

Tatzelt, C., Henning, S., Welti, A., Baccarini, A., Hartmann, M., Gysel-Beer, M., van Pinxteren, M., Modini, R. L., Schmale, J., and Stratmann, F.: Circum-Antarctic abundance and properties of CCN and INPs, Atmos. Chem. Phys., 22, 9721–9745, https://doi.org/10.5194/acp-22-9721-2022, 2022.

Tobo, Y., Adachi, K., DeMott, P. J., Hill, T. C. J., Hamilton, D. S., Mahowald, N. M., Nagatsuka, N., Ohata, S., Uetake, J., Kondo, Y., and Koike, M.: Glacially sourced dust as a potentially significant source of ice nucleating particles, Nat. Geosci., 12, 253–258, https://doi.org/10.1038/s41561-019-0314-x, 2019.

Tornow, F., Ackerman, A. S., and Fridlind, A. M.: Preconditioning of overcast-to-broken cloud transitions by riming in marine cold air outbreaks, Atmos. Chem. Phys., 21, 12049–12067, https://doi.org/10.5194/acp-21-12049-2021, 2021.

U.S. National Ice Center, Fetterer, F., Savoie, M., S., H., and Clemente-Colón, P.: Multisensor Analyzed Sea Ice Extent – Northern Hemisphere (MASIE-NH), Version 1, National Snow and Ice Data Center [data set], https://doi.org/10.7265/N5GT5K3K, 2010.

Vali, G.: Quantitative Evaluation of Experimental Results an the Heterogeneous Freezing Nucleation of Supercooled Liquids, J. Atmos. Sci., 28, 402–409, https://doi.org/10.1175/1520-0469(1971)028<0402:QEOERA>2.0.CO;2, 1971.

Vali, G.: Revisiting the differential freezing nucleus spectra derived from drop-freezing experiments: methods of calculation, applications, and confidence limits, Atmos. Meas. Tech., 12, 1219–1231, https://doi.org/10.5194/amt-12-1219-2019, 2019.

Vergara-Temprado, J., Murray, B. J., Wilson, T. W., O'Sullivan, D., Browse, J., Pringle, K. J., Ardon-Dryer, K., Bertram, A. K., Burrows, S. M., Ceburnis, D., DeMott, P. J., Mason, R. H., O'Dowd, C. D., Rinaldi, M., and Carslaw, K. S.: Contribution of feldspar and marine organic aerosols to global ice nucleating particle concentrations, Atmos. Chem. Phys., 17, 3637–3658, https://doi.org/10.5194/acp-17-3637-2017, 2017.

Vergara-Temprado, J., Miltenberger, A. K., Furtado, K., Grosvenor, D. P., Shipway, B. J., Hill, A. A., Wilkinson, J. M., Field, P. R., Murray, B. J., and Carslaw, K. S.: Strong control of Southern Ocean cloud reflectivity by ice-nucleating particles, P. Natl. Acad. Sci. USA, 115, 2687–2692, https://doi.org/10.1073/pnas.1721627115, 2018.

Wegener, A.: Thermodynamik der Atmosphäre, J. A. Barth, Leipzig, 1911.

Wendisch, M., Crewell, S., Ehrlich, A., Herber, A., Kirbus, B., Lüpkes, C., Mech, M., Abel, S. J., Akansu, E. F., Ament, F., Aubry, C., Becker, S., Borrmann, S., Bozem, H., Brückner, M., Clemen, H.-C., Dahlke, S., Dekoutsidis, G., Delanoë, J., De La Torre Castro, E., Dorff, H., Dupuy, R., Eppers, O., Ewald, F., George, G., Gorodetskaya, I. V., Grawe, S., Groß, S., Hartmann, J., Henning, S., Hirsch, L., Jäkel, E., Joppe, P., Jourdan, O., Jurányi, Z., Karalis, M., Kellermann, M., Klingebiel, M., Lonardi, M., Lucke, J., Luebke, A. E., Maahn, M., Maherndl, N., Maturilli, M., Mayer,

B., Mayer, J., Mertes, S., Michaelis, J., Michalkov, M., Mioche, G., Moser, M., Müller, H., Neggers, R., Ori, D., Paul, D., Paulus, F. M., Pilz, C., Pithan, F., Pöhlker, M., Pörtge, V., Ringel, M., Risse, N., Roberts, G. C., Rosenburg, S., Röttenbacher, J., Rückert, J., Schäfer, M., Schaefer, J., Schemann, V., Schirmacher, I., Schmidt, J., Schmidt, S., Schneider, J., Schnitt, S., Schwarz, A., Siebert, H., Sodemann, H., Sperzel, T., Spreen, G., Stevens, B., Stratmann, F., Svensson, G., Tatzelt, C., Tuch, T., Vihma, T., Voigt, C., Volkmer, L., Walbröl, A., Weber, A., Wehner, B., Wetzel, B., Wirth, M., and Zinner, T.: Overview: quasi-Lagrangian observations of Arctic air mass transformations – introduction and initial results of the HALO–(AC)3 aircraft campaign, Atmos. Chem. Phys., 24, 8865–8892, https://doi.org/10.5194/acp-24-8865-2024, 2024.

Wex, H., Huang, L., Zhang, W., Hung, H., Traversi, R., Becagli, S., Sheesley, R. J., Moffett, C. E., Barrett, T. E., Bossi, R., Skov, H., Hünerbein, A., Lubitz, J., Löffler, M., Linke, O., Hartmann, M., Herenz, P., and Stratmann, F.: Annual variability of ice-nucleating particle concentrations at different Arctic locations, Atmos. Chem. Phys., 19, 5293–5311, https://doi.org/10.5194/acp-19-5293-2019, 2019.

Whale, T. F., Murray, B. J., O'Sullivan, D., Wilson, T. W., Umo, N. S., Baustian, K. J., Atkinson, J. D., Workneh, D. A., and Morris, G. J.: A technique for quantifying heterogeneous ice nucleation in microlitre supercooled water droplets, Atmos. Meas. Tech., 8, 2437–2447, https://doi.org/10.5194/amt-8-2437-2015, 2015.

Williams, A. S., Dedrick, J. L., Russell, L. M., Tornow, F., Silber, I., Fridlind, A. M., Swanson, B., DeMott, P. J., Zieger, P., and Krejci, R.: Aerosol size distribution properties associated with cold-air outbreaks in the Norwegian Arctic, Atmos. Chem. Phys., 24, 11791–11805, https://doi.org/10.5194/acp-24-11791-2024, 2024.

Wilson, T. W., Ladino, L. A., Alpert, P. A., Breckels, M. N., Brooks, I. M., Browse, J., Burrows, S. M., Carslaw, K. S., Huffman, J. A., Judd, C., Kilthau, W. P., Mason, R. H., McFiggans, G., Miller, L. A., Nájera, J. J., Polishchuk, E., Rae, S., Schiller, C. L., Si, M., Temprado, J. V., Whale, T. F., Wong, J. P. S., Wurl, O., Yakobi-Hancock, J. D., Abbatt, J. P. D., Aller, J. Y., Bertram, A. K., Knopf, D. A., and Murray, B. J.: A marine biogenic source of atmospheric ice-nucleating particles, Nature, 525, 234–238, https://doi.org/10.1038/nature14986, 2015.

Xi, Y., Xu, C., Downey, A., Stevens, R., Bachelder, J. O., King, J., Hayes, P. L., and Bertram, A. K.: Ice nucleating properties of airborne dust from an actively retreating glacier in Yukon, Canada, Environmental Science: Atmospheres, 2, 714–726, https://doi.org/10.1039/D1EA00101A, 2022.

Yang, X., Pyle, J. A., and Cox, R. A.: Sea salt aerosol production and bromine release: Role of snow on sea ice, Geophys. Res. Lett., 35, L16815, https://doi.org/10.1029/2008GL034536, 2008.

Young, G., Jones, H. M., Darbyshire, E., Baustian, K. J., McQuaid, J. B., Bower, K. N., Connolly, P. J., Gallagher, M. W., and Choularton, T. W.: Size-segregated compositional analysis of aerosol particles collected in the European Arctic during the ACCACIA campaign, Atmos. Chem. Phys., 16, 4063–4079, https://doi.org/10.5194/acp-16-4063-2016, 2016.

Zhao, X., Huang, K., Fu, J. S., and Abdullaev, S. F.: Long-range transport of Asian dust to the Arctic: identification of transport pathways, evolution of aerosol optical properties, and impact assessment on surface albedo changes, Atmos. Chem. Phys., 22, 10389–10407, https://doi.org/10.5194/acp-22-10389-2022, 2022.